

# Galaxy Groups at $0.3 \leq z \leq 0.55$ . I. Group Properties

D. J. Wilman<sup>1,2,6</sup>, M. L. Balogh<sup>1,3</sup>, R. G. Bower<sup>1</sup>, J. S. Mulchaey<sup>4</sup>,  
 A. Oemler Jr<sup>4</sup>, R. G. Carlberg<sup>5</sup>, S. L. Morris<sup>1</sup>, R. J. Whitaker<sup>1</sup>

<sup>1</sup>Physics Department, University of Durham, South Road, Durham DH1 3LE, U.K.

<sup>2</sup>Max-Planck-Institut für extraterrestrische Physik, Giessenbachstraße, D-85748 Garching, Germany (present address)

<sup>3</sup>Department of Physics, University of Waterloo, Waterloo, Ontario, Canada N2L 3G1 (present address).

<sup>4</sup>Observatories of the Carnegie Institution, 813 Santa Barbara Street, Pasadena, California, U.S.A.

<sup>5</sup>Department of Astronomy, University of Toronto, Toronto, ON, M5S 3H8 Canada.

<sup>6</sup>email: dwilman@mpe.mpg.de

9 October 2018

## ABSTRACT

The evolution of galaxies in groups may have important implications for the evolution of the star formation history of the universe, since many processes which operate in groups may suppress star formation and the fraction of galaxies in bound groups grows rapidly between  $z = 1$  and the present day. In this paper, we present an investigation of the properties of galaxies in galaxy groups at intermediate redshift ( $z \sim 0.4$ ). The groups were selected from the CNOC2 redshift survey as described in Carlberg et al. (2001), with further spectroscopic follow-up undertaken at the Magellan telescope in order to improve the completeness and depth of the sample. We present the data for the individual groups, and find no clear trend in the fraction of passive galaxies with group velocity dispersion and group concentration. We stack the galaxy groups in order to compare the properties of group galaxies with those of field galaxies at the same redshift. The groups contain a larger fraction of passive galaxies than the field, this trend being particularly clear for galaxies brighter than  $M_{B_J} < -20$  in the higher velocity dispersion groups. In addition, we see evidence for an excess of bright passive galaxies in the groups relative to the field. In contrast, the luminosity functions of the star forming galaxies in the groups and the field are consistent. These trends are qualitatively consistent with the differences between group and field galaxies seen in the local universe.

**Key words:** galaxies:fundamental parameters – galaxies:evolution – galaxies:stellar content – catalogues

## 1 INTRODUCTION

Clusters of galaxies have received intensive observational study over the last decades. This effort has lead to clear results on the way galaxy properties, such as morphology and star formation rate, vary within clusters and how these properties evolve between clusters at different redshifts (Dressler 1980; Butcher & Oemler 1984; Dressler et al. 1997; Poggianti et al. 1999, see Bower & Balogh 2004 for a recent review). In contrast, comparably-detailed studies of galaxy groups and their evolution have only recently begun in earnest. The group environment is likely to have a significant impact on star formation rates in the member galaxies (Zabludoff & Mulchaey 1998; Hashimoto et al. 1998; Tran et al. 2001) and recent work has emphasised that even for galaxies now in rich clusters, much of the transformation of the galaxies' properties may have taken place in groups embedded in the filamentary structure (Kodama et al. 2001; Balogh et al.

2004). In addition, while few galaxies in the local universe are located in clusters, up to 50 per cent (Huchra & Geller 1982; Eke et al. 2004) may be located in galaxy groups. Furthermore, this number is strongly redshift-dependent, as a larger and larger fraction of galaxies become members of groups as the large-scale structure of the universe develops. Thus the properties of galaxies in groups and the impact of the group environment on the evolution of galaxies can have an important bearing on the decline of the cosmic star formation rate from  $z = 1$  to the present-day (Lilly et al. 1996; Madau et al. 1998; Hopkins 2004).

Studies of nearby groups show that their galaxy populations exhibit properties which vary from cluster-like (mostly early-type) to field-like (mostly late type) (Zabludoff & Mulchaey 1998). However we know that groups span a wide range in local density, upon which the morphological composition (Postman & Geller 1984; Zabludoff & Mulchaey 1998; Tran et al. 2001) and the mean star forming proper-

ties (Hashimoto et al. 1998; Balogh et al. 2004) strongly depend (e.g. Dressler 1980; Postman & Geller 1984; Hashimoto et al. 1998; Gómez et al. 2003; Balogh et al. 2004; Kauffmann et al. 2004). The wide range of galaxy populations found in nearby groups is likely to be a natural consequence of these correlations. Conversely, the powerful dependence of galaxy properties on local densities typical of groups suggests that groups provide the ideal environment for galaxy transformations. This may result in the strong dependence of early type fraction and passive dwarf galaxy abundance on group velocity dispersion and X-ray luminosity, observed in nearby groups (Zabludoff & Mulchaey 1998, 2000; Christlein 2000). In particular, galaxy interactions are expected to be common in groups, in which the velocity dispersion is typically not much larger than that of the constituent galaxies (Hashimoto et al. 1998; Severgnini & Saracco 2001).

Groups have a much lower density contrast against the background galaxy population, so most work has concentrated on groups which are either unusually compact (Hickson et al. 1989) or X-ray luminous (Mulchaey et al. 2003). More recently, the advent of large field galaxy redshift surveys has made it possible to study galaxy groups selected purely on the basis of their three dimensional galaxy density. In the local universe, early redshift surveys and more recently the extensive 2dF Galaxy Redshift Survey (2dFGRS) and Sloan Digital Sky Survey (SDSS) have generated large group catalogues which can be used as the basis for studies of galaxies in the group environment (Huchra & Geller 1982; Ramella et al. 1989, 1997, 1999; Hashimoto et al. 1998; Tucker et al. 2000; Martínez et al. 2002; Eke et al. 2004; Balogh et al. 2004). However, the properties of higher redshift groups have been relatively little explored. This is largely because of the difficulty in finding suitable systems, and the low success rate of spectroscopic follow-up of group members. Allington-Smith et al. (1993) used radio galaxies to preselect groups in order to study the evolution of the blue galaxy fraction with redshift, while Carlberg et al. (2001) have presented a group catalogue based on the CNOC2 galaxy redshift survey.

In this paper, we present new data obtained in the region of 26 CNOC2 groups at  $0.3 \leq z \leq 0.55$  with LDSS2 on Magellan. In Sections 2 and 3 we introduce the data and explain why we have chosen to use the [OII] emission line to study statistical trends in star formation. In Section 4 we begin by describing the data reduction procedure and our method for determination of redshifts and emission line equivalent widths for each galaxy. Section 4.3 then goes on to explain our procedure for group membership allocation. In Section 5 we present the properties of the 26 individual groups in order to examine any trends of structural group properties with star formation. Finally, in Section 6 groups are stacked to enable detailed statistical analysis, and we investigate the link between the group environment and star formation by contrasting the stacked group with our sample of field galaxies selected from the same redshift range.

In a second paper (Wilman et al. 2004, hereafter known as Paper II), we present a comparison of the star forming properties of these intermediate redshift groups with local groups selected from the 2PIGG catalogue at  $0.05 \leq z \leq 0.1$  (Eke et al. 2004).

Throughout this paper we assume a  $\Lambda$ CDM cosmology of  $\Omega_M = 0.3$ ,  $\Omega_\Lambda = 0.7$  and  $H_0 = 75 \text{ km s}^{-1} \text{ Mpc}^{-1}$ .

## 2 CNOC2 GROUPS

### 2.1 The survey

The second Canadian Network for Observational Cosmology Redshift Survey (CNOC2) was recently completed with the aim of studying galaxy clustering in the redshift range  $0.1 < z < 0.6$  (Yee et al. 2000; Shepherd et al. 2001). The CNOC2 survey is split into 4 patches, approximately equally spaced in RA and totalling 1.5 square degrees in area. The survey consists of 5 colour  $UBVR_CI_C$  photometry with  $\sim 4 \times 10^4$  galaxies down to the photometric limit  $R_C = 23.0$ . The MOS spectrograph on the CFHT 3.6m telescope was used to obtain spectra for over  $\sim 6000$  galaxies in total, 48 per cent complete down to  $R_C = 21.5$ . Combination of the imaging and spectroscopy lead to a very well determined selection function for the spectroscopic sample (Yee et al. 2000) and comparisons with our deeper spectroscopy suggest that brighter than this limit the CNOC2 survey is not biased towards emission line objects. The transmission efficiency of the band limiting filter and grism combination was above half power in the wavelength range  $4387 - 6285 \text{ \AA}$ , effectively limiting the redshift range of the survey. The most prominent absorption features (Ca II H and K) lie in this wavelength range for galaxies in the redshift range  $0.12 < z < 0.58$ , whereas either the [OII] or [OIII] emission lines fall in this wavelength range for all galaxies in the range  $0 < z < 0.68$ .

### 2.2 The CNOC2 groups

Distant groups have always been difficult to recognize because of their sparse galaxy populations. The presence of high redshift groups has typically been inferred indirectly via the presence of a radio galaxy or X-ray emitting intragroup medium (IGM, Allington-Smith et al. 1993; Jones et al. 2002). Whilst these surveys provide a useful insight into the evolution of galaxy properties in rich galaxy groups, the selection criteria strongly bias the selection towards these richer elliptical dominated groups, whereas low redshift samples point to a more numerous population of low density, X-ray faint, spiral dominated groups (Mulchaey et al. 2003).

The CNOC2 survey provided a powerful opportunity to generate a kinematically selected sample of galaxy groups. A friends-of-friends percolation algorithm was used to detect groups of galaxies in redshift space. This was followed by a trimming step in which a centre, velocity dispersion,  $\sigma_1$  and  $r_{200}$  ( $\sim$  virial radius) were estimated and then members were added or deleted within  $3 \times \sigma_1$  and  $1.5 \times r_{200}$  in 3 rounds of iteration (see Carlberg et al. 2001). A total sample of over 200 galaxy groups was detected. Although the spectroscopic sample is incomplete, this group sample represents a kinematically selected sample at intermediate redshifts ( $0.12 < z < 0.55$ ), free from the strong biases present in samples selected by other means.

### 2.3 Deeper LDSS2 data

We used the Multi-Object Spectrograph LDSS2 (Low Dispersion Survey Spectrograph) on the 6.5m Baade Telescope at Las Companas Observatory (LCO) in Chile to obtain a deeper and more complete sample of galaxies in the region

of 20 of the CNOC2 groups at  $0.3 \leq z \leq 0.55$  located in the 3 out of 4 CNOC2 patches accessible from the latitude of LCO. Masks were designed using an automated selection algorithm to minimise selection bias and maximise the allocation of targets per mask. Due to the proximity on the sky of some of the CNOC2 groups, the masks were chosen to serendipitously sample a further 11 groups from the Carlberg et al. (2001) sample, although only 6 of these lie at  $z > 0.3$ . Targets were prioritised using an automated algorithm which favours brighter objects and objects which lie close together along the mask's spectral axis. This second criterion ensures that the spectral coverage does not vary wildly from object to object in each mask. The data were taken in 4 separate observing runs between May 2001 and November 2002. Each LDSS2 mask covers approximately  $6.5' \times 5'$  and in the CNOC2 fields it is normal to fit between 20 and 30 slits onto a mask. Between 1 and 3 masks were observed per target group, depending upon the density of target galaxies in that area of sky. Mask exposures varied from 1 to 4 hours depending on the phase of the moon and observing conditions. For maximum throughput, the blue-optimised medium resolution grism was used with a dispersion of  $5.3\text{\AA}$  (on the fourth run the red optimised grism was used which has the same dispersion and similar efficiency at wavelengths of interest). The slits have a width =  $1.47''$  which corresponds to  $8.78\text{\AA}$  of spectral coverage (compared to  $6.28\text{\AA}$  in the original CNOC2 masks). Using the CNOC2 photometric classifier from the CNOC2 photometric catalogue, we targeted 634 objects classified as *galaxies*, 102 objects classified as *possible galaxies*. Where there were free spaces on the mask with no galaxies present, we allocated 130 objects classified as *probable stars*. From this last category, 29 out of 130 objects had galaxy-like spectra which yielded redshifts. The remaining 101 were correctly identified as stars. Included in our targets were 35 galaxies which already had redshifts from the initial CNOC2 survey. These were reobserved to form a comparison sample which is used to understand the accuracy of our measurements.

In Table 1 we show the number of galaxies targetted in each field and the serendipitous Carlberg et al. (2001) groups which lie in these fields.

### 3 MEASUREMENT OF STAR FORMATION USING EW[OII]

To study the relative levels of star formation in statistical galaxy samples, we use the  $[\text{OII}]\lambda 3727$  emission line which lies centrally in the visible window in our CNOC2 redshift range of  $0.3 \leq z \leq 0.55$  and at wavelengths of low sky emission. At  $z > 0.21$ , the  $\text{H}\alpha$  emission line disappears entirely from the LDSS2 spectrograph window with the instrument sensitivity dropping in the red with the current optics and detector. Furthermore, at  $z \gtrsim 0.1$  measurements of  $\text{H}\alpha$  are compromised by the increase in sky line density with increasing wavelength. Hopkins et al. (2003) have recently shown using data from local galaxies in SDSS that measurements of SFR using [OII] emission are consistent with those from  $\text{H}\alpha$  and 1.4GHz luminosities. Also the scatter in the  $\text{H}\alpha$ -[OII] relationship is primarily luminosity dependent (Jansen et al. 2001) and so in a given luminosity range the systematic error in using the [OII] measurement to infer star formation

**Table 1.** The number of galaxies targetted in each targetted group and the  $0.3 \leq z \leq 0.55$  Carlberg et al. (2001) groups serendipitous in these fields.

Targetted Group	Number of targetted galaxies	Serendipitous Carlberg et al. (2001) groups
22	24	23,33
24	45	8
25	48	none
28	86	none
31	38	none
32	20	13
34	55	none
37	24	1,27,35
38	48	40
39	88	23,33
134	47	132,138
137	52	140
138	54	129,132,133,134
139	28	none
140	62	137
227	53	none
228	19	none
232	24	241
241	14	201,232
244	37	243

rates is significantly reduced. Additionally, even at  $z < 1$ , Flores et al. (2004) place the contribution from dusty starburst galaxies to the total SFR, underestimated by optical emission line measurements at  $\lesssim 20$  per cent. Rather than inferring star formation rates, we deliberately limit our study to direct comparison between [OII] measurements to avoid model dependency in our results. Finally, we restrict our analysis to EW[OII] rather than [OII] flux and star formation rates. Normalisation by the continuum reduces uncertainties related to absorption by dust and aperture bias as well as providing a measure of SFR per unit luminosity.

## 4 DATA PROCESSING

### 4.1 Data Reduction

We extracted and calibrated our spectra using mainly IRAF tools in the *onedspec* and *twodspec* packages. Wavelength calibration was applied using both IRAF tools and new MOS reduction software written by Dan Kelson in Carnegie (Kelson 2003). We have tested both these methods to ensure that consistent solutions are obtained. The wavelength calibration is based upon arcs taken during daytime and is secure in the wavelength range  $3700\text{\AA} \leq \lambda \leq 8000\text{\AA}$  which corresponds to  $z \leq 2.1$  for the [OII] emission line and  $z \leq 0.6$  for [OIII] which extends far beyond the redshift range of interest. Around bright skylines, systematic residuals often remain. We interpolated over these regions.

To account for mismatch between the daytime arc and nighttime science observations, we then applied a zero point offset to the wavelength calibration. This is computed by measuring the offset of the  $5577\text{\AA}$  skyline in the arc-calibrated frames. Most of these offsets were  $< 5\text{\AA}$  and we

did not detect any significant non-linearities. The new wavelength solution appears robust, as evidenced in the comparison of LDSS2 and CNOC2 redshifts (see Figure 1 which is explained in Section 4.2.2).

## 4.2 Redshift Measurement

The IRAF tool *xcsao* in the *rvsao* package (Kurtz & Mink 1998) was used to cross-correlate all the spectra with templates of rest-frame early-type (absorption line) and late-type (emission line) galaxies. The early-type galaxy template was created by coadding a large number of high signal to noise early type galaxy spectra from the sample, each of which had been shifted to zero redshift.<sup>1</sup> The emission line (Sc) template is a high signal to noise spectrum of NGC4775 from the atlas of Kennicutt (1992) and smoothed to the resolution of LDSS2.<sup>2</sup> We shall henceforth refer to redshifts obtained using the late-type template as *emission* redshifts and those obtained using the early-type template as *absorption* redshifts.

The peak in the cross-correlation spectrum is selected by *xcsao* to give an estimate of the redshift for each object (Tonry & Davis 1979). To assess redshift measurements, redshifts attained using the early-type (absorption) and late-type (emission) templates were assessed in each case by manually inspecting the spectra and assigning a redshift quality flag. The quality assessment is based upon the number of believable emission lines in an emission line spectrum. In absorption line spectra, we simply decide whether to accept or reject a solution. For example, a solution with a visible 4000Å break would be accepted. Spectra containing a single emission line received further checks to ensure the emission is real. Finally, redshifts which became apparent upon visual inspection were applied by setting up that solution as the initial guess in *rvsao*. However, if no peak in the cross-correlation spectrum could be obtained at the correct redshift then the solution was abandoned.

The final redshift of a target was selected by comparing the redshift quality flag from emission and absorption redshifts. Where the absorption and emission redshifts agree within errors, emission redshifts are preferred due to their greater accuracy. However, where the emission redshift was not secure and a different, higher quality absorption redshift exists, then the absorption redshift is used. Objects with no acceptable redshift are discounted from the spectroscopic sample.

In total we have 418 redshifts from the LDSS2 data of which 240 are in the range  $21 \leq R_c \leq 22$  which dramatically improves the completeness at this depth. In the whole sample, we have 86 new group members from LDSS2 spectroscopy. This increases the total group sample to 295 in 26 groups (see Group Membership section for further details of group allocation). In the magnitude range  $21 \leq R_c \leq 22$  and

<sup>1</sup> High signal to noise early type galaxy spectra used to create our template are shifted to zero redshift by cross-correlation with a high signal to noise spectrum of NGC3379 from the atlas of Kennicutt (1992).

<sup>2</sup> Velocity zero points of both Kennicutt (1992) spectral templates have been improved to an accuracy of  $30 \text{ km s}^{-1}$  (Yee et al. 1996).

within  $150''$  of targeted group centres, we obtained 179 additional redshifts (36 members) on top of the 115 (27 members) existing from the CNOC2 survey. We consider  $R_c = 22$  to be our magnitude limit at which we can obtain redshifts for  $\sim 60$  per cent of objects targeted; our success rate for all targeted galaxies brighter than  $R_c = 22$  is 74 per cent. The selection functions are well understood and targeted galaxies for which we do not manage to obtain a redshift are evenly distributed in colour, suggesting that our sample is unbiased (see Appendix A).

### 4.2.1 Emission Line Equivalent Width Measurements

We measure the [OII] equivalent widths using our own purpose written code to compare the flux in two separate continuum regions with that in a feature bandpass. We use the definition from Dressler & Shectman (1987) for [OII], in which the feature bandpass ranges from 3718Å to 3738Å and the continua regions have width 65Å adjacent to the line region on either side.

### 4.2.2 Comparison with CNOC2 data

In Figure 1 we compare the redshift and EW[OII] measurements obtained from the LDSS2 spectra and the CNOC2 spectra, for objects in common to both surveys. It can be seen that the redshifts from the two surveys are generally in good agreement. Out of 35 galaxies with redshifts from both sources, only four of the redshifts are discrepant. Three of these are faint objects ( $B > 23.5$ ,  $R_c > 21.5$ ). We also examine the combined spectral signal (total counts, *cts*) from the wavelength ranges 5300Å–5530Å and 5645Å–5820Å which span the most efficient region of the grism, eliminating the strong night sky lines (as used to examine targets for which no redshifts were measured in Appendix A2). These three objects all fall in the low signal range ( $cts < 1.5 \times 10^4$ ) along with 8 of the remaining 32 galaxies in the combined sample. We exclude the three discrepant redshifts for faint, low signal objects from the figure. The other discrepant redshift is offset by  $\sim 800 \text{ km s}^{-1}$  (rest-frame). Inspection shows that the LDSS2 redshift provides a better fit to the emission lines. Of the remaining 31 galaxies in this sample, the standard deviation of the rest-frame velocity offsets ( $(cz_{CNOC2} - cz_{LDSS2})/(1+z)$ ),  $\Delta(v)_{tot} = 175 \text{ km s}^{-1}$  with a mean value of only  $-6 \text{ km s}^{-1}$ . To check the dependence of rest-frame velocity offsets on the spectral counts, we also show the distribution for the 14 galaxies with  $cts < 2.25 \times 10^4$  (dashed histogram). We find no correlation, amongst these remaining objects, between spectral signal strength and velocity offset.

Using duplicate observations Yee et al. (2000) show that the random rest-frame velocity errors in the CNOC2 redshifts is  $103 \text{ km s}^{-1}$ . As the typical velocity difference in our common-object sample is  $175 \text{ km s}^{-1}$ , we compute an approximate rest-frame error on LDSS2 spectra of  $\Delta(v)_{LDSS2} = \sqrt{175^2 - 103^2} = 142 \text{ km s}^{-1}$ . We expect that the velocity errors are dominated by the CNOC2 astrometrical errors of  $\lesssim 1''$  (Yee et al. 2000). Indeed the errors computed using the common-object sample are consistent with an rms astrometrical error of  $\sim 0.25''$ .

In the right hand panel of Figure 1, we show that measurements of EW[OII] in LDSS2 spectra (measured using

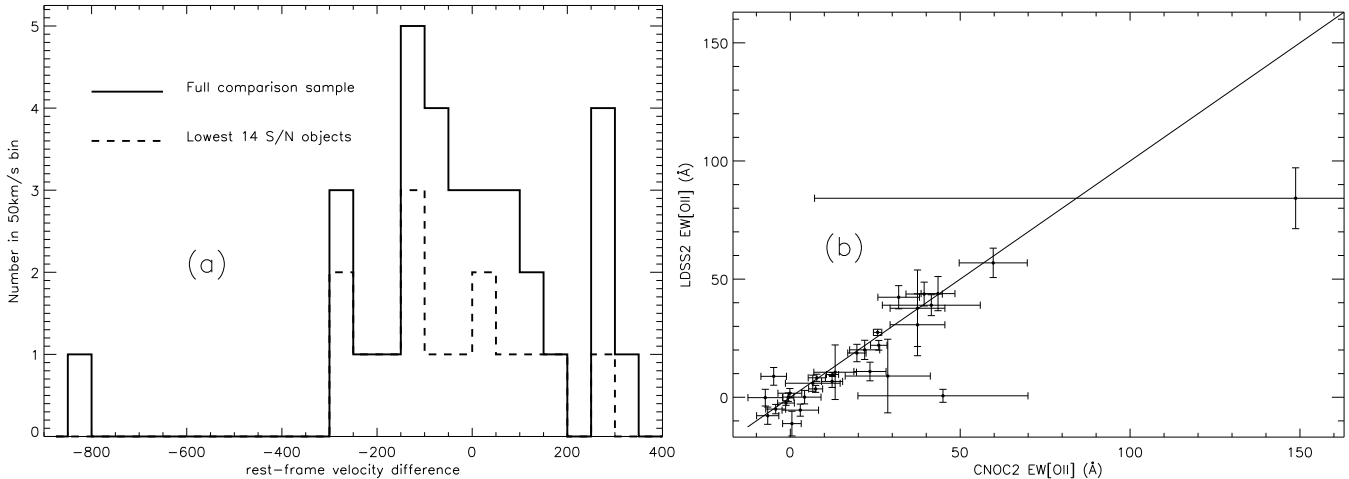


**Figure 1.** A comparison of velocity and EW[OII] measurements in CNOC2 and LDSS2 measurements using the 31 galaxies with matched redshifts in the comparison sample. (a): The distribution of rest-frame velocity offset,  $(cz_{CNOC2} - cz_{LDSS2})/(1+z)$ , in all galaxies (solid line) and the 14 galaxies with the lowest combined signal in the wavelength ranges 5300Å–5530Å and 5645Å–5820Å (dashed line, see text for more detail). and (b): Comparison between rest-frame EW[OII] measurements, for the galaxies in which redshifts and EW[OII] have been obtained from LDSS2 spectra *and* in the original CNOC2 catalogue.

our code) are also in excellent agreement with the original CNOC2 survey measurements (Whitaker et al. 2004) within errors, showing that our measurements are consistent with CNOC2. The code used for both sets of measurements is essentially the same and tests show that they provide identical results.

### 4.3 Group Membership

To obtain a consistently selected sample of galaxy groups, we restricted ourselves to examining those groups which were pre-selected from the sample of Carlberg et al. (2001) and targetted with LDSS2 on Magellan. This provides a sample of 26 targetted and serendipitous Carlberg et al. (2001) groups in the range  $0.3 \leq z \leq 0.55$ . We derive from the virial theorem  $r_{200} \sim \sigma(v)[11.5H_{75}(z)]^{-1}$  where  $\sigma(v)$  is the velocity dispersion and  $H_{75}(z)$  is the Hubble constant at the group redshift  $z$  and  $H_{75}(0) = 75 \text{ km s}^{-1} \text{ Mpc}^{-1}$ . This means that a group with  $\sigma(v) = 300 \text{ km s}^{-1}$  has  $r_{200} = 0.28h_{75}^{-1} \text{ Mpc}$  at  $z = 0.4$ , with  $r_{200}$  scaling with  $\sigma(v)$ . The group finding algorithm of Carlberg et al. (2001) was tuned to identify dense, virialized groups of 3 members or more with the goal of tracing the properties of the underlying dark matter halos. With this in mind, a conservative linking-length ( $0.33h_{75}^{-1} \text{ Mpc}$ ) and trimming radius of  $1.5r_{200}$  in the spatial axes of the groups were selected.

Our objectives differ from those of Carlberg et al. (2001) in that we wish to understand the global properties of galaxies in groups, not only those galaxies in the virialized core regions. In order to be more representative of the loose group population, whilst retaining the strict selection criteria of Carlberg et al. (2001), we choose to relax the projected trimming radius for group members in our redefined group sample. In effect, we find that relaxing this parameter allows the more compact groups to retain the same membership whilst other groups gain extra members.

Although defining the contents of a group is a subjective problem, there exist some tools which make the task easier.

Peculiar motion of galaxies moving in a gravitational potential artificially lengthens the group along the line-of-sight direction in redshift space (the finger-of-God effect). From the virial theorem, one can make the assumption that the projected spatial and line-of-sight dimensions of a group in redshift space are approximately in constant proportion (in rest-frame coordinates). Eke et al. (2004) show that an axial ratio of  $\sim 11$  for the length along the line of sight relative to the projected spatial length is most appropriate for a linking volume in a friends-of-friends algorithm. Interlopers in redshift space are difficult to identify and eliminate, so we choose a conservative line-of-sight trimming radius of twice the velocity dispersion.

We choose a small aspect ratio of  $b = 3.5$ , to compute our trimming radius. Although this will exceed  $r_{200}$ , it results in a stable membership solution for all 26 groups and allows us to examine how radial trends within the groups extend to the group outskirts and infall regions (see Section 6.1.1). However most of our analysis will be conducted within a fixed metric group aperture. We note that these results are insensitive to the choice of a particular value of  $b$ , as large as 11.

The algorithm for defining the final membership of each group in our sample works as follows:

- The group is initially assumed to be located at the latest position in redshift space determined by Carlberg et al. (2001)<sup>3</sup> with an initial observed-frame velocity dispersion,  $\sigma(v)_{obs}$ , of 500 km s<sup>-1</sup>.
- The redshift range required for group membership is computed from equation 1, which limits membership in the line-of-sight direction to within twice the velocity dispersion:

$$\delta(z)_{max} = 2 \frac{\sigma(v)_{obs}}{c} \quad (1)$$

- This is converted into a spatial distance,  $\delta(\theta)_{max}$ , which corresponds to a redshift space distance related to the distance computed in the line-of-sight direction by the aspect ratio,  $b$ .  $\delta(\theta)_{max}$  is computed as:

$$\delta(\theta)_{max} = 206265'' \cdot \left[ \frac{\delta(r)_{max}}{h_{75}^{-1} \text{Mpc}} \right] \cdot \left( \frac{D_\theta}{h_{75}^{-1} \text{Mpc}} \right)^{-1} \quad (2)$$

where  $D_\theta$ , the angular diameter distance in physical coordinates, is a function of  $z$ , and

$$\delta(r)_{max} = \frac{c\delta(z)_{max}}{b(1+z)H_{75}(z)} \quad (3)$$

with  $b = 3.5$ .

- Group members are selected by applying the redshift and positional limits  $\delta(z) = |z - z_{group}| \leq \delta(z)_{max}$  and the angular distance from the group centre,  $\delta(\theta) \leq \delta(\theta)_{max}$ .
- We recompute the observed velocity dispersion of the group,  $\sigma(v)_{obs}$ , using the Gapper algorithm (equation 4) which is insensitive to outliers and thus gives an accurate estimate of the velocity dispersion for small groups (Beers et al. 1990):<sup>4</sup>

$$\sigma(v)_{obs} = 1.135c \times \frac{\sqrt{\pi}}{n(n-1)} \sum_{i=1}^{n-1} w_i g_i \quad (4)$$

with  $w_i = i(n-i)$  and  $g_i = z_{i+1} - z_i$ .

- We also redefine the centre of the group, taking the luminosity weighted centroid in projected spatial coordinates and the mean redshift to be the new group centre.
- We then recompute the limiting redshift offset  $\delta(z)_{max}$  and positional offset  $\delta(\theta)_{max}$  using equations 1, 2 and 3. The galaxies are then reassigned to the group as before.

- The whole process is repeated until a stable membership solution is reached. In all 26 groups such a stable solution is found, mostly within 2 iterations although the massive group 138 requires 4 iterations. We finally compute the rest-frame velocity dispersion (equation 5) and the intrinsic velocity dispersion. The latter is computed by combining the measurement errors of the component galaxies (equation 6) and removing in quadrature from the measured velocity dispersion (equation 7).

<sup>3</sup> Note: these positions have been updated since publication

<sup>4</sup> The multiplicative factor 1.135 corrects for the 2 $\sigma$  clipping of a gaussian velocity distribution.

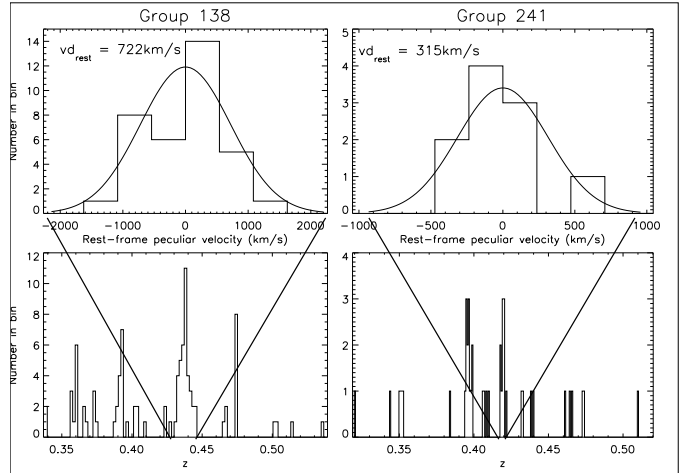


**Figure 2.** Bottom: Redshift distributions in the regions of two groups; Top: Velocity distribution of the group members; The smooth line represents a gaussian with  $\sigma = \sigma(v)_{obs}$ .

$$\sigma(v)_{rest} = \frac{\sigma(v)_{obs}}{1+z} \quad (5)$$

$$\langle \Delta(v) \rangle^2 = \frac{1}{N} \sum_{i=1}^N \Delta(v)_i^2 \quad (6)$$

where  $\Delta(v) = 142$  km s<sup>-1</sup> (LDSS2)  
and  $\Delta(v) = 103$  km s<sup>-1</sup> (CNOC2)

$$\sigma(v)_{intr}^2 = \sigma(v)_{rest}^2 - \langle \Delta(v) \rangle^2 \quad (7)$$

The combined velocity errors ( $\langle \Delta(v) \rangle$ ) in group 24 exceed the measured velocity dispersion  $\sigma(v)_{rest}$  and so we compute an upper limit to the intrinsic velocity dispersion using Monte-Carlo simulations. With  $\sigma(v)_{intr} = 119.6$  km s<sup>-1</sup> in 15.87 per cent of iterations a value of  $\sigma(v)_{rest}$  less than the measured value is obtained from the simulations, corresponding to the 1 $\sigma$  value of a one tailed gaussian. Errors on  $\sigma(v)_{intr}$  are computed in all other groups using the Jackknife technique (Efron 1982). We note that in groups with few known members (e.g. group 40) the true error on  $\sigma(v)_{intr}$  may be underestimated using this technique.

In Figure 2, we show velocity histograms for two of our groups and the redshift space clustering in the region of those groups. The left-hand panels show the rich group 138, possibly even a poor cluster, whilst the right-hand panels show the medium-sized group 241. The overplotted Gaussian of width  $\sigma(v)_{obs}$  provides a good envelope to the distribution in both cases, which is typical of all 26 groups. We further note that there is no significant trend of velocity dispersion with redshift in our sample indicating that we do not preferentially select higher mass groups at higher redshift (where the survey does not probe so far down the luminosity function).

Whilst group members lie some distance (up to  $\sim 4.5r_{200}$ ) from the group centre and are included in the cal-

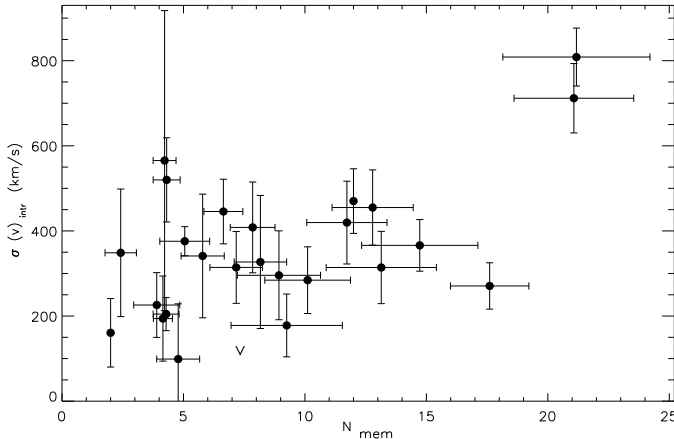


**Figure 3.** Intrinsic velocity dispersion of galaxy groups,  $\sigma(v)_{intr}$  plotted against the number of galaxy members within 1 Mpc and brighter than  $M_{B_J} = -20$ , corrected for incompleteness ( $N_{mem}$ ). Errors on  $N_{mem}$  represent the Poisson error on the number of candidate members estimated to lie in the group (see Section 4.3 for definition).

culation of the velocity dispersion, we limit our analysis to galaxies inside a  $1h_{75}^{-1}$  Mpc projected radius at the group redshift ( $\sim 3.5r_{200}$  for a group with  $\sigma(v)_{intr} = 300$  km  $s^{-1}$ ), where we understand the completeness (see Appendix A). Rest-frame  $B_J$  luminosities are determined to minimise the K-corrections (the  $B_J$ -band well matches the  $R_c$  selection band at the redshift of CNOC2 galaxies) and to allow easy comparison with the properties of the 2dFGRS local galaxy population (see Paper II for more detail on determination of K-corrections). Luminosities include a correction for Galactic extinction on a patch-to-patch basis, computed by extrapolating from B and V band extinction values obtained from NED (Schlegel et al. 1998, variation within each patch is negligible). A luminosity  $M_{B_J} = -20$  approximates the magnitude limit,  $R_c = 22$  for most galaxies at  $z = 0.55$ . We compute  $N_{mem}$ , an estimate of the number of group members brighter than  $M_{B_J} = -20$  and within  $1h_{75}^{-1}$  Mpc projected distance from the group centre.  $N_{mem}$  is the sum of the number of known members and candidate members (the number of galaxies without redshifts which are predicted to lie at the group redshift, and which would meet our luminosity and radial cuts). Figure 3 shows  $N_{mem}$  plotted against the intrinsic velocity dispersion  $\sigma(v)_{intr}$  of each group. Any weak correlation between  $N_{mem}$  and  $\sigma(v)_{intr}$  is largely masked by a good deal of scatter (excluding the two largest systems). This scatter might be attributed to the variation in group structure and the difficulty of obtaining accurate estimates of velocity dispersion with few members. Limiting the membership to galaxies within  $0.5h_{75}^{-1}$  Mpc projected radius does not reduce the scatter in this relationship.

## 5 INDIVIDUAL GROUP ANALYSIS

### 5.1 Basic Parameters

In Table 2 we present some of the fundamental properties of our CNOC2 group sample including the velocity dispersion,  $\sigma(v)_{intr}$  and the number of members of each group (both the

total with measured redshifts,  $N_{tot}$ , and the number brighter than  $M_{B_J} = -20$  and within  $1h_{75}^{-1}$  Mpc of the group centre, weighted to account for incompleteness,  $N_{mem}$ ). The group *class* and parameter  $f_p$  is defined in Section 5.2. Groups closer to the low redshift limit of  $z = 0.3$  are on average complete down to fainter luminosities. Incompleteness over the full luminosity range is also a function of the fraction of targeted objects in the group vicinity.

### 5.2 Star Formation in the CNOC2 groups

The local galaxy population shows a distinct bimodality in galaxy properties. This is seen in galaxy colours (Strateva et al. 2001; Blanton et al. 2003; Baldry et al. 2004) and in  $EW[H\alpha]$  (Balogh et al. 2004). In Section 6.1 and Paper II we shall show that an artificial division in  $EW[OII]$  at  $5\text{\AA}$  is sufficient to reveal trends in the fraction of star-forming galaxies ( $EW[OII] \geq 5\text{\AA}$ ) and passive galaxies ( $EW[OII] < 5\text{\AA}$ ) in the stacked group. We also create a third category of objects, the highly star-forming galaxies, with  $EW[OII] \geq 30\text{\AA}$ . The spatial distribution of these three types of objects in our 26 groups reveals the connection between star formation and the local environment of galaxies within each group. Figures 4 and 5 show the spatial distribution of these three types of galaxy in our 26 groups, ordered by their velocity dispersion  $\sigma(v)_{intr}$ . At our high redshift limit of  $z = 0.55$ , galaxies brighter than our magnitude limit  $R_c = 22$  possess luminosities of  $M_{B_J} \lesssim -20$ . Therefore group members brighter than this luminosity (luminous members) are represented by larger symbols, while faint members ( $M_{B_J} > -20$ ) are represented by smaller symbols. A limiting radius for our LDSS2 targeting is typically  $\sim 240''$ , which corresponds to  $1h_{75}^{-1}$  Mpc at the low redshift end of our sample,  $z = 0.3$ . We represent the  $1h_{75}^{-1}$  Mpc radius centred on the luminosity-weighted centroid of all known members in each group, with an overplotted circle. We also compute an iteratively defined centre by throwing out galaxies beyond  $1h_{75}^{-1}$  Mpc and recomputing the luminosity-weighted centroid. This is repeated twice, reducing the radial limit to  $0.75h_{75}^{-1}$  Mpc and finally to  $0.5h_{75}^{-1}$  Mpc. A  $0.5h_{75}^{-1}$  Mpc radius circle ( $\sim r_{200}$  for a  $\sigma(v)_{intr} = 500$  km  $s^{-1}$  group) centred on this iteratively defined centre is also shown. Finally, it is pertinent to recognise that a small fraction of galaxies in close proximity to the group centre but without redshifts may also be members. Such galaxies which would have luminosities  $M_{B_J} \leq -20$  should they lie at the group redshift are overplotted as crosses. We refer to these galaxies as candidate luminous members.

As can be seen in Figures 4 and 5, groups come in all shapes and sizes. Judgement about global group properties is reserved for the stacked group which smoothes out the peculiarities of each individual group. This is covered in Section 6 and Paper II. Some general trends are nonetheless readily apparent in Figures 4 and 5:

- Some of the groups show clumps of either passive or star forming galaxies. The clumps of passive galaxies would be expected from the star formation - density relation (Balogh et al. 2004). However, the clumps of star forming galaxies (seen for example in groups 244, 133, 232) could represent a part of the group system which had not been influenced by the group environment at the redshift of these groups.

**Table 2.** Individual group properties: Luminosity-weighted group centroid positions in spatial coordinates (columns 2,3); mean redshift (column 4); velocity dispersion,  $\sigma(v)_{intr}$  (column 5); total number of galaxies in each group with a redshift,  $N_{tot}$  (column 6); the number of members brighter than  $M_{B_J} = -20$  and within  $1h_{75}^{-1}$ Mpc, weighted to account for incompleteness,  $N_{mem}$  (column 7); the group morphology classification (column 8); the luminosity of the brightest group galaxy (within  $1h_{75}^{-1}$ Mpc of the centre),  $M_{B_J}(Br)$ , (column 9); and the fraction of passive galaxies in the group,  $f_p$  (brighter than  $M_{B_J} = -20.0$  and within  $0.5h_{75}^{-1}$ Mpc of the iteratively determined group centre, column 10) The computation of  $f_p$  includes resampling to account for galaxies without redshifts in the region of each group (See Section 5.2.2).

Group	RA (J2000)	Dec (J2000)	z	$\sigma(v)_{intr}$ (km s $^{-1}$ )	$N_{tot}$	$N_{mem}$	Class	$M_{B_J}(Br)$	$f_p$
23	14:49:25.0	+09:30:26	0.351	445 $\pm$ 75	13	6.64	C	-21.84	0.67
24	14:49:03.9	+09:06:57	0.359	<119.6	11	7.33	C	-21.7	0.71
25	14:49:40.8	+09:13:43	0.361	470 $\pm$ 75	19	12.00	C	-21.17	0.63
27	14:49:49.9	+09:06:38	0.372	348 $\pm$ 149	8	2.41	L	-22.35	1.00
28	14:50:22.8	+09:01:13	0.372	160 $\pm$ 80	6	2.00	C	-20.47	1.00
31	14:49:12.9	+09:10:09	0.392	565 $\pm$ 352	5	4.22	L	-21.06	0.33
32	14:50:01.3	+08:55:57	0.394	519 $\pm$ 98	9	4.30	L	-21.05	0.25
33	14:49:36.8	+09:28:48	0.406	194 $\pm$ 100	7	4.15	L	-20.98	0.80
34	14:48:43.8	+08:52:02	0.465	408 $\pm$ 106	11	7.84	L	-21.71	0.25
37	14:49:29.1	+09:05:33	0.471	419 $\pm$ 97	19	11.72	C	-21.66	1.00
38	14:49:27.8	+08:58:12	0.510	808 $\pm$ 68	19	21.17	M	-22.58	0.29
39	14:49:23.2	+09:30:24	0.536	454 $\pm$ 88	15	12.78	C	-22.41	0.88
40	14:49:20.2	+08:54:57	0.542	177 $\pm$ 73	4	9.25	U	-21.04	0.33
129	21:51:03.3	-05:42:23	0.317	225 $\pm$ 76	7	3.90	C	-20.98	0.50
132	21:50:25.8	-05:40:53	0.359	375 $\pm$ 34	9	5.05	L	-21.02	1.00
133	21:50:48.2	-05:37:33	0.373	204 $\pm$ 38	4	4.28	U	-20.41	0.00
134	21:50:24.8	-05:41:29	0.392	284 $\pm$ 78	12	10.11	L	-20.99	0.33
137	21:50:37.7	-05:29:18	0.425	314 $\pm$ 84	8	7.17	C	-22.27	1.00
138	21:50:48.2	-05:39:53	0.437	711 $\pm$ 81	35	21.07	M	-21.83	1.00
139	21:50:25.8	-05:50:20	0.439	314 $\pm$ 84	12	13.14	L	-21.69	0.71
140	21:50:41.4	-05:28:38	0.465	98 $\pm$ 129	5	4.78	C	-21.78	0.33
227	02:26:29.5	+00:12:08	0.363	341 $\pm$ 145	7	5.78	L	-21.49	0.33
228	02:25:05.7	-00:07:12	0.384	326 $\pm$ 156	8	8.16	C	-21.66	0.67
232	02:25:50.7	+00:52:17	0.396	366 $\pm$ 60	14	14.72	C	-21.81	0.29
241	02:25:58.7	+00:54:21	0.419	295 $\pm$ 104	10	8.93	L	-21.38	0.43
244	02:25:45.0	+01:07:30	0.470	270 $\pm$ 54	18	17.60	C	-22.20	0.10

- Passive galaxies are not restricted to the most centrally concentrated, isolated groups and the most massive groups. They are also present in loose and filamentary groups.

### 5.2.1 Trends with group concentration

Figures 4 and 5 show the wide variety of group structures present in the intermediate-age Universe, from low  $\sigma(v)_{intr}$  compact groups (e.g. groups 24 and 28), and more massive groups spanning the gap to poor-clusters (groups 38 and 138) to elongated structures (group 232) and loose groups (e.g. groups 33 and 34). Incompleteness makes the application of any strict quantifiable compactness parameter to the groups difficult. However, for the purpose of studying basic trends in galaxy properties with the overall group structure, we divide the groups into three qualitative but readily identifiable categories, hereafter known as the group class. These categories are concentrated (C), loose (L) and massive (M). Groups which cannot be classified are labelled unclassifiable, (U). The more massive groups 38 and 138 are class M, identifying the more cluster-like environment in these richer groups ( $\sigma(v)_{intr} \geq 600$  km s $^{-1}$  and  $N_{mem} \geq 20$ ). Groups in which galaxies are located in dense clumps (and therefore biased towards higher density in, for example, the morphology-density relation) are classified as class C. More loosely clustered groups are classified as class L and groups 40 and 133 are not classified at all (class U) as each possesses only 4 confirmed members with no structure readily apparent. The class of each group is shown in Table 2.

We wish to see how the concentration of group galaxies

(i.e. the group structure or state of virialisation) might affect the underlying star forming properties of the group galaxies. In Figure 6, we show the distributions of EW[OII] in the C-group galaxies (solid histogram) and L-group galaxies (dotted histogram; renormalised to match the number of C-group galaxies). Galaxies are limited to within  $0.5h_{75}^{-1}$ Mpc of the iteratively determined group centre (smaller circles in Figures 4 and 5). In the top panel, galaxies are limited to  $M_{B_J} \leq -20.0$  and in the bottom panel we include all group galaxies down to  $M_{B_J} \leq -18.5$ . The EW[OII] distribution of the L-group galaxy population is well matched to the C-group galaxy population (as confirmed by a K-S test). We ensure that this result is unchanged when the luminosity distributions of the two samples are exactly matched, using a resampling technique. This involves choosing an L-group galaxy closely matching the luminosity of each C-group galaxy, which results in some L-group galaxies being chosen more than once and others not at all. The dashed histogram in Figure 6 represents the resampled L-group galaxy EW[OII] distribution. The resampling process has negligibly altered the L-group galaxy EW[OII] distribution which is still therefore consistent with the C-group galaxy population.

Dividing the galaxies once more on their EW[OII] into passive galaxies ( $EW[OII] < 5\text{\AA}$ ), star forming galaxies ( $5\text{\AA} \leq EW[OII] \leq 30\text{\AA}$ ) and highly star forming galaxies ( $EW[OII] \geq 30\text{\AA}$ ), we can take the fraction of galaxies in each category directly from Figure 6. Table 3 shows the fraction of passive galaxies,  $f_p$ , and the fraction of highly star-forming galaxies,  $f_{hsf}$ , in both the C-group galaxy pop-

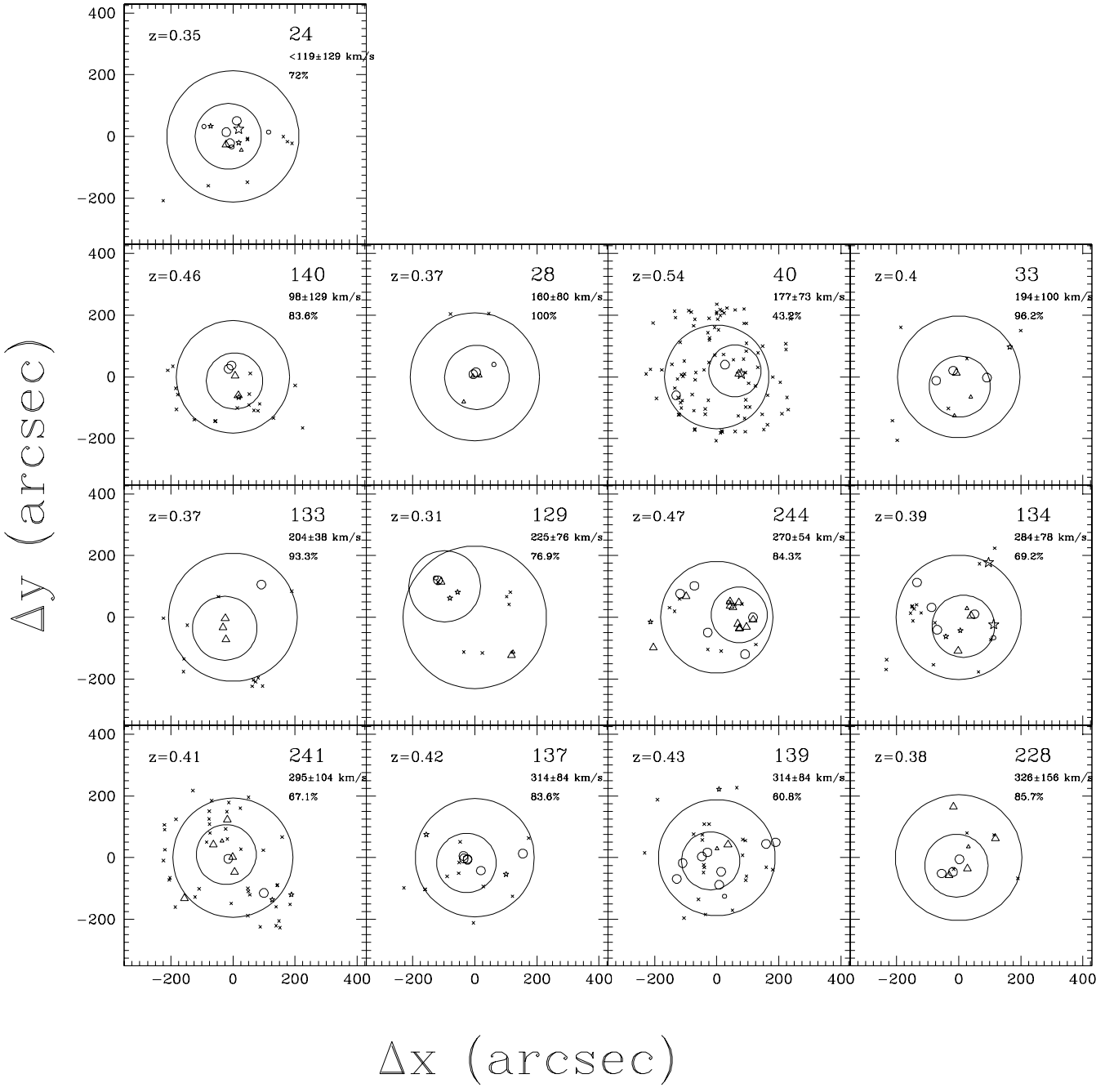


**Figure 4.** The 13 groups with lowest  $\sigma(v)_{intr}$  Passive galaxies, star forming galaxies and highly star forming galaxies are represented by *circles*, *triangles* and *stars* respectively. Luminous members are represented by larger symbols than faint members. *Crosses* represent candidate luminous members. These are bright galaxies without measured redshifts and, while in some groups these will be mostly foreground galaxies, in other groups (preferentially the more massive ones) a significant number may also be group members. The  $1h_{75}^{-1}$  Mpc radius of each group is also shown centred on the luminosity-weighted centre computed using all known members. We also show a  $0.5h_{75}^{-1}$  Mpc radius circle centred on an iteratively defined centre (see Section 5.2). Definitions of these galaxy types can be found in the text (Section 5.2). With each group, we also display the group redshift, velocity dispersion  $\sigma(v)_{intr}$  and completeness within  $1h_{75}^{-1}$  Mpc and brighter than the  $R_c$ -band magnitude required for the galaxy to have a luminosity  $M_{B_J} \leq -20$  should the galaxy be at the group redshift. Completeness is a function of redshift and the fraction of targeted objects in the group vicinity. Note that groups are ordered by velocity dispersion,  $\sigma(v)_{intr}$ .

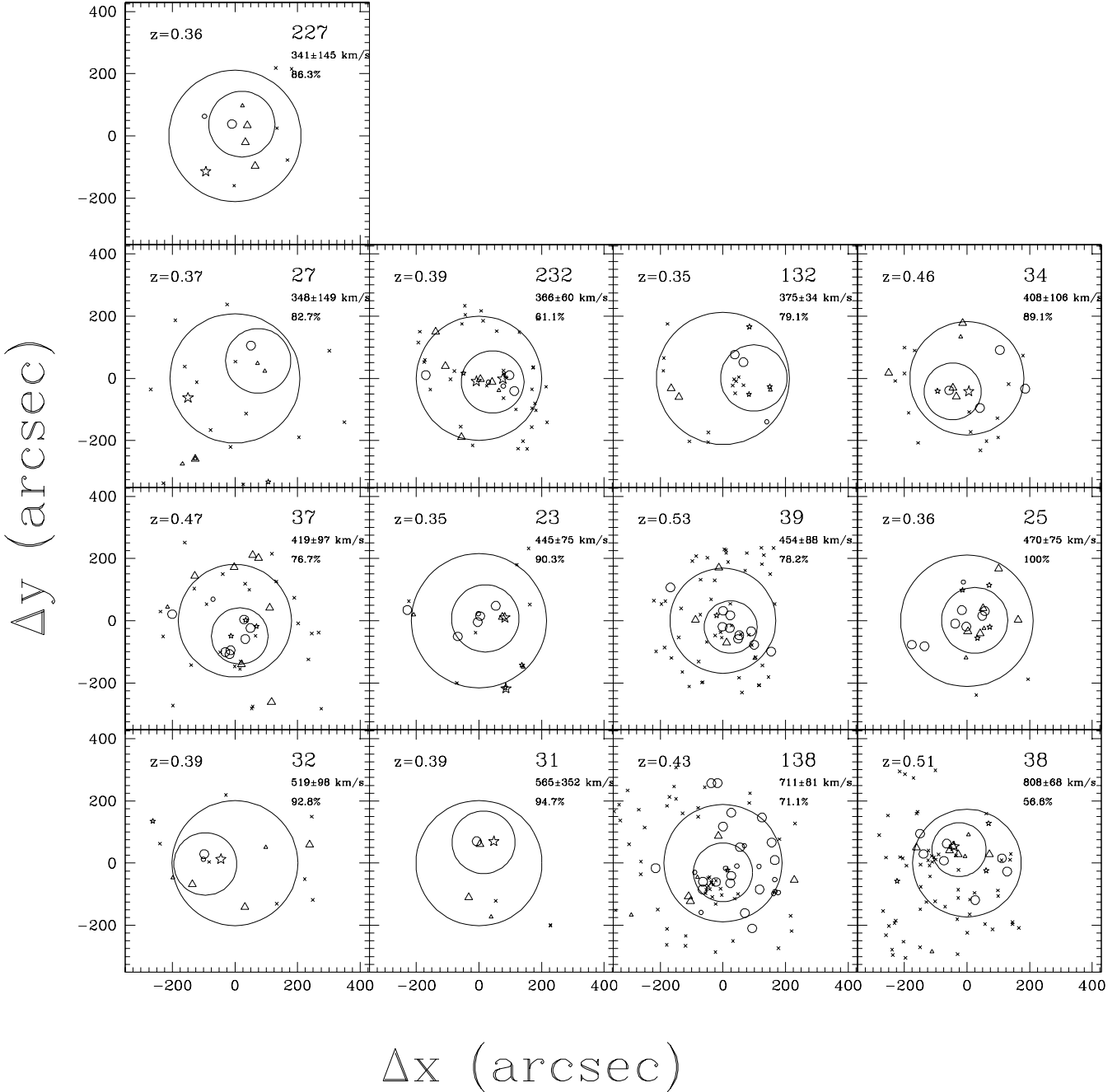


**Figure 5.** As Figure 4 for the 13 groups with highest  $\sigma(v)_{intr}$ .

ulation, and the L-group galaxy population (raw and resampled) with both luminosity limits applied. We note that the small differences between the two classes (less passive and more highly star forming galaxies in the loose groups) are not significant, and that these figures should not be overinterpreted as the group classification is uncertain.

#### 5.2.2 Trends with group velocity dispersion

The value of  $f_p$  in each group is computed for all known group galaxies within  $0.5h_{75}^{-1}\text{Mpc}$  of the iteratively determined group centre and brighter than  $M_{B_J} = -20.0$ . We also include candidate members in the sample (see Section 4.3 for

definition). For each candidate member we assign the properties (redshift,  $\text{EW}[\text{OII}]$ ) of a galaxy with a measured redshift and a similar  $(B - R_C)$  colour and  $R_C$  magnitude (referred to as a measured- $z$  galaxy). This galaxy must also lie in the projected region of the group, and a galaxy 0.5 mags different in  $R_C$  is considered an equally good match to one 0.25 mags different in  $(B - R_C)$  colour. In this way a high redshift group (where a  $M_{B_J} = -20.0$  galaxy has  $R_C \sim 22.0$ ) is evenly sampled in luminosity despite incompleteness at faint magnitudes. Nonetheless, we find that every group  $f_p$  is consistent with the value computed from known members only. Values of  $f_p$  for each group are also shown in Table 2.  $f_p$  is plotted against group velocity dispersion,  $\sigma(v)_{intr}$  in

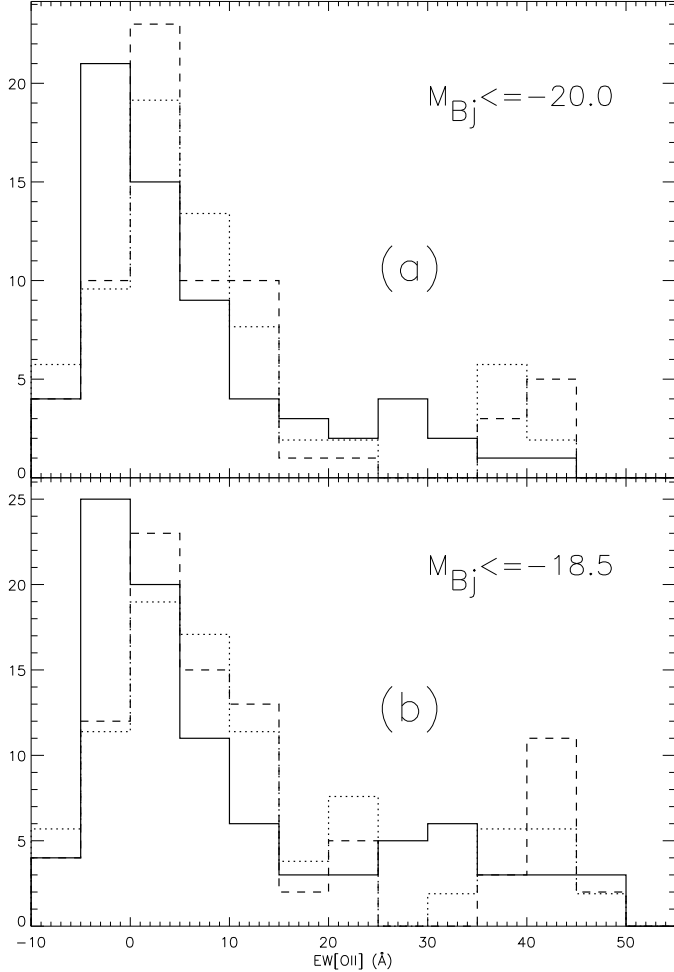


**Figure 6.** (a) The distribution of  $\text{EW}[\text{OII}]$  for the C-group galaxies (solid histogram), L-group galaxies (dotted histogram, renormalized to match the number of C-group galaxies) and the L-group galaxies, resampled to match the luminosity distribution of galaxies in the concentrated groups (dashed histogram). The sample is limited to galaxies brighter than  $M_{B_J} \leq -20.0$  and to within  $0.5h_{75}^{-1}\text{Mpc}$  of the iteratively determined group centre (smaller circles in Figures 4 and 5). (b) The same as above, except incorporating all galaxies down to the fainter limit of  $M_{B_J} \leq -18.5$ .

**Table 3.** The fractions of passive ( $f_p$ ,  $\text{EW}[\text{OII}] < 5\text{\AA}$ ) and highly star forming ( $f_{\text{hsf}}$ ,  $\text{EW}[\text{OII}] \geq 30\text{\AA}$ ) galaxies in C-group galaxies (concentrated into dense clumps), L-group galaxies (looser structure) and resampled L-group galaxies (to match the luminosity distribution of C-group galaxies). Galaxy populations are defined within  $0.5h_{75}^{-1}\text{Mpc}$  of the iteratively determined group centre and down to  $M_{B_J} = -20.0$  (1) and  $M_{B_J} = -18.5$  (2). Statistical errors are computed using the Jackknife technique.

Class	$f_p$ (1)	$f_{\text{hsf}}$ (1)	$f_p$ (2)	$f_{\text{hsf}}$ (2)
C	$61 \pm 6\%$	$6 \pm 6\%$	$53 \pm 5\%$	$16 \pm 7\%$
L	$51 \pm 9\%$	$11 \pm 5\%$	$39 \pm 7\%$	$18 \pm 4\%$
Resampled L	$55 \pm 6\%$	$12 \pm 6\%$	$42 \pm 5\%$	$20 \pm 5\%$

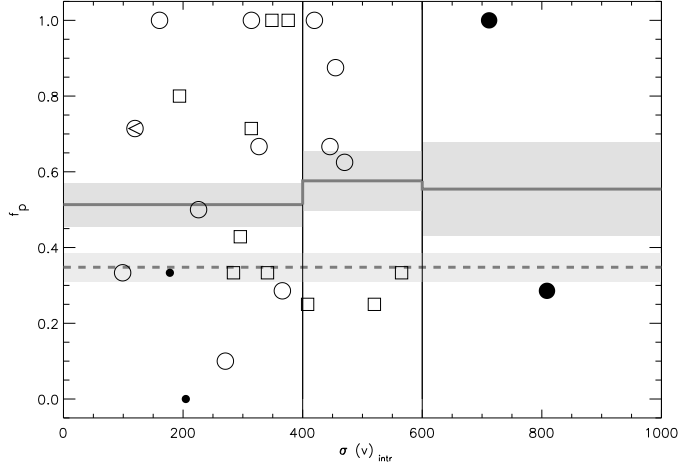


**Figure 7.** The fraction of passive galaxies  $f_p$  (brighter than  $M_{B_J} \leq -20.0$  and within  $0.5h_{75}^{-1}\text{Mpc}$  of the iteratively determined group centre), in each group as a function of the group velocity dispersion,  $\sigma(v)_{\text{intr}}$ . The galaxies in each group without redshift measurement (candidate members) are resampled from the measured- $z$  galaxies in the same region of sky, on the basis of their luminosity and  $(B - R_c)$  colour. Groups are also keyed on the allocated group-class with *open circles* to represent concentrated groups, *squares* to represent loose groups, *large filled circles* to represent massive groups and *small filled circles* to represent unclassified groups. The arrow indicates an upper limit on the velocity dispersion of group 28. We also show the value of  $f_p$  in combined groups for three bins of  $\sigma(v)_{\text{intr}}$  (*solid line*) and for the field (*dotted line*). The *shaded area* represents the  $1\sigma$  error on these values computed using the Jackknife technique. There is no clear trend of  $f_p$  with  $\sigma(v)_{\text{intr}}$  in groups for galaxies brighter than  $M_{B_J} \leq -20.0$ .

Figure 7. Groups are also keyed on their class. There is no clear trend of  $f_p$  with  $\sigma(v)_{\text{intr}}$  and the scatter in the individual values is large because of the small number of galaxies in each group. In order to improve the statistics in this plot, we bin the groups in velocity dispersion. The average  $f_p$  in each bin shows no systematic evidence for variation with  $\sigma(v)_{\text{intr}}$ . In general, there is little trend of  $f_p$  with group class. Only for systems with  $\sigma(v)_{\text{intr}} > 400 \text{ km s}^{-1}$  velocity dispersion is there a suggestion that the concentrated groups have higher  $f_p$  than the loose systems. We note that  $f_p$  also shows no correlation with group redshift within the sample.

## 6 THE STACKED GROUP

We have shown that there are no significant differences between groups of different class or velocity dispersion, so we now consider their properties when combined. We co-add the data from our 26 groups to form a stacked group. We then possess the statistical tools necessary to investigate the global properties of group galaxies and to make a comparison with the field at intermediate redshift ( $0.3 \leq z \leq 0.55$ ). The stacked group sample contains a total of 282 galaxies above our magnitude limit of  $R_C = 22.0$ . Each galaxy is weighted by a combined selection weight  $W_C$  to correct for the stacked group selection functions. These are well understood and are discussed in detail in Appendix A. However, we only trust the weights when applied to a large sample as

incompleteness varies from group to group. Whilst the application of this weight is strictly correct, we find the results from Section 6.1 are consistent with and without the galaxy weightings.

We also define a field sample to contrast with our stacked group sample. Field galaxies are defined to include all galaxies not associated with the Carlberg et al. (2001) group sample, with  $0.3 \leq z \leq 0.55$  and within  $240''$  of the targetted group centre (where the radial selection function is well defined). The field sample contains a total of 334 galaxies above our magnitude limit of  $R_C = 22.0$ .

### 6.1 The properties of stacked group galaxies

In this section we investigate how galaxy properties in the stacked group differ from the field population.

#### 6.1.1 The fraction of passive galaxies in the stacked group

In Figure 8 we show how the fraction of passive galaxies,  $f_p$ , depends upon galaxy  $B_J$ -band luminosity in the stacked group and the field. This should be distinguished from  $f_p$  computed for each individual group in Section 5 and Figure 7. In the top panel of Figure 8, we limit the group sample to galaxies within  $0.5h_{75}^{-1}$  Mpc of the iteratively determined group centre (corresponding to  $r_{200}$  for  $\sigma(v)_{intr} \sim 500 \text{ km s}^{-1}$  groups). There is a clear enhancement of  $f_p$  in the group galaxies with respect to the field, especially in the luminosity range  $-22.0 \leq M_{B_J} \leq -19.0$ . In the lower panel, we include all galaxies within  $1h_{75}^{-1}$  Mpc of the original centroid computed in Section 4.3 (the luminosity-weighted centre of all confirmed group members). There is no significant change in  $f_p$  as a function of luminosity when the radial constraint is relaxed, apart from an improvement in the sample statistics. Combining all galaxies within the luminosity range  $-22.5 \leq M_{B_J} \leq -18.5$ , the enhancement in groups of  $f_p$  is better than  $3\sigma$  significance, and this trend is still evident if the massive groups 38 and 138 are excluded from the sample. However we note that brighter than  $M_{B_J} = -21.0$  the value of  $f_p$  is only enhanced in groups of higher velocity dispersion ( $\sigma(v)_{intr} \gtrsim 400 \text{ km s}^{-1}$ ). During the remainder of our analysis we limit the galaxy sample to those within  $1h_{75}^{-1}$  Mpc from the luminosity-weighted centre of all confirmed group members.

In the top panel of Figure 9, we plot  $f_p$  as a function of group-centric radius  $\delta(r)$  for all group galaxies brighter than  $M_{B_J} = -18.5$ . We have used a physical distance scale since virial radii in groups are uncertain due to the low number of galaxies and often irregular group morphologies. The horizontal solid line and dashed lines represent the field  $f_p$  and  $\pm 1\sigma$  uncertainties respectively. There is a weak trend of  $f_p$  with  $\delta(r)$  and a significant enhancement over the field is seen out to  $1.0h_{75}^{-1}$  Mpc. The lack of strong trend is unsurprising: the groups are not relaxed, spherical systems and often have multiple concentrations within the fiducial  $1.0h_{75}^{-1}$  Mpc radius (see Figures 4 and 5). To see if any trend becomes more obvious when the group is centred on the BGG (Brightest Group Galaxy, chosen from within  $1h_{75}^{-1}$  Mpc of the luminosity-weighted group centre), we recalculate the radial trend placing the group centre on the BGG. This enhances  $f_p$  in the innermost bin, but does

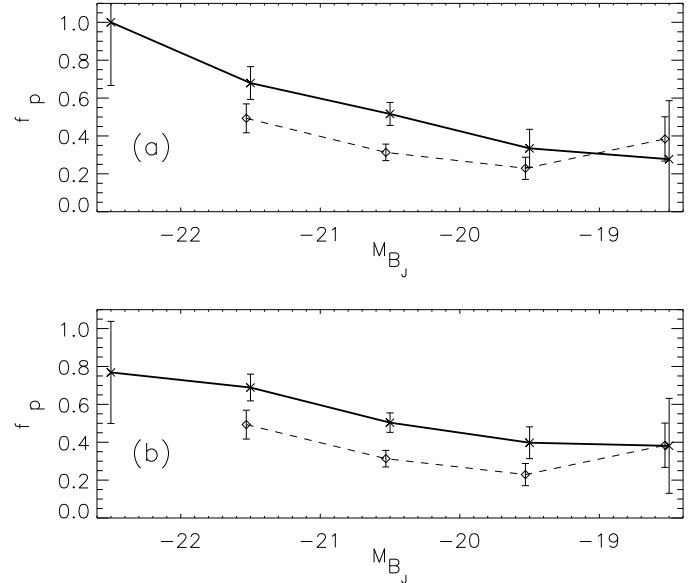


**Figure 8.** (a): The fraction of passive galaxies,  $f_p$ , in the stacked group within  $0.5h_{75}^{-1}$  Mpc of the iteratively determined group centre (solid line) and the field (dashed line) as a function of galaxy luminosity,  $M_{B_J}$ . The field symbols are offset slightly in luminosity for clarity. Statistical errors on  $f_p$  are computed using a Jackknife method. (b): The same as above, but including all galaxies within  $1h_{75}^{-1}$  Mpc of the original centroid computed in Section 4.3 (the luminosity-weighted centre of all confirmed group members).

not otherwise strengthen the radial gradient. In Figure 10 we show the dependence of  $f_p$  on the distance to the nearest confirmed group galaxy. This measure of density has the advantage that it can be applied to systems with few members and irregular spatial distribution. In this plot,  $f_p$  is significantly reduced at large separations, indicating that the high passive fraction seen in Figure 10 at large  $\delta(r)$  is related to the clumpy distribution of group galaxies. We note, however that there is no dependence on separation less than  $\sim 0.4h_{75}^{-1}$  Mpc.

#### 6.1.2 Environmental dependencies in the luminosity function of galaxies

In Figure 11 we show how the luminosity function of the stacked group (solid histogram) compares with that of the field (dashed histogram) over the same redshift range ( $0.3 \leq z \leq 0.55$ ). For a full discussion of evolution in the CNOC2 field luminosity function, see Lin et al. (1999); here we concentrate on the comparison with the groups. The field luminosity function has been scaled to match the number of galaxies seen in the group luminosity function over the range  $-21.0 \leq M_{B_J} \leq -20.0$ . The vertical line represents the luminosity limit of galaxies where  $R_c = 22.0$  at  $z = 0.55$  ( $M_{B_J} = -19.75$ ), our high redshift limit, for galaxies with mean K-corrections. At the low redshift limit  $z = 0.3$  the corresponding luminosity limit is  $M_{B_J} = -17.93$ . For the galaxies with the largest K-corrections, these limits become  $M_{B_J} = -18.06$  at  $z = 0.3$  and  $M_{B_J} = -20.07$  at  $z = 0.55$ . Figure 11 suggests that there may be a small excess of bright ( $M_{B_J} \leq -21.0$ ) galaxies in the groups with respect to the field.

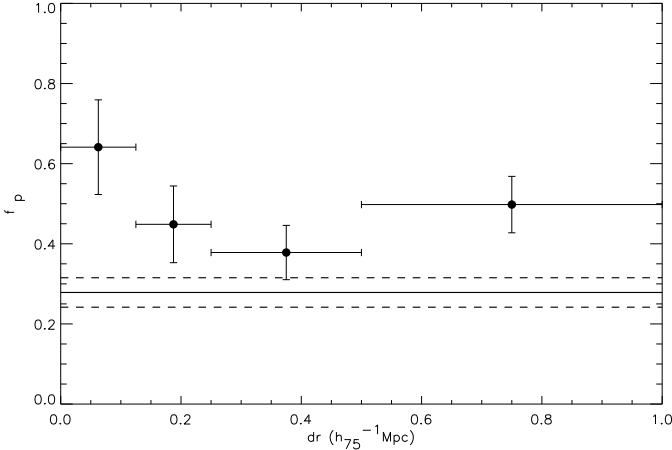


**Figure 9.**  $f_p$  ( $M_{B_J} \leq -18.5$ ) in the stacked group as a function of physical distance from the group centre where the group centre is defined to be the luminosity-weighted centre of all confirmed group members. The horizontal solid line and dashed lines represent the field  $f_p$  and  $\pm 1\sigma$  uncertainties respectively (The luminosity limit is deeper than in Figure 7 and so  $f_p$  is reduced). All errors on  $f_p$  are computed using the Jackknife method.

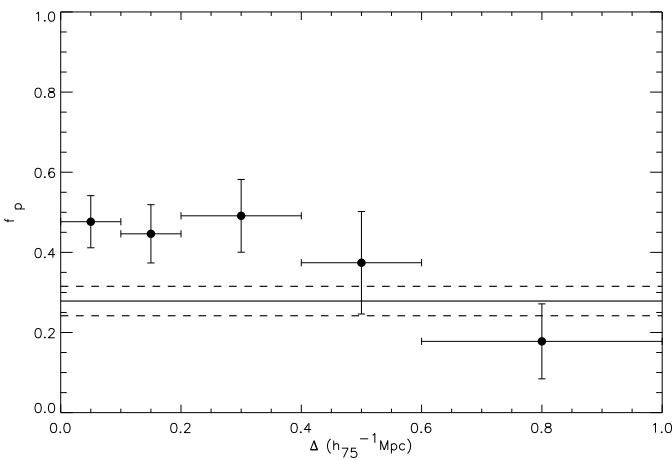


**Figure 10.**  $f_p$  ( $M_{B_J} \leq -18.5$ ) in the stacked group as a function of the projected distance to the nearest neighbour ( $\Delta h_75^{-1}$  Mpc). The horizontal solid line and dashed lines represent the field  $f_p$  and  $\pm 1\sigma$  uncertainties respectively. All errors on  $f_p$  are computed using the Jackknife method. We find a correlation between  $f_p$  and  $\Delta$  where group galaxies located in more overdense regions ( $\Delta \lesssim 0.4 h_75^{-1}$  Mpc) have an enhanced likelihood of being passive.

A concern with this comparison is that the field galaxies have a different redshift distribution from the group galaxies. This is a particular concern at the faint end of the luminosity function where the selection effect has the greatest impact. In order to see if this can account for the difference between the field and group luminosity functions, we apply an additional weighting to the field galaxies to match the redshift distribution of the group galaxies. The luminosity functions of the redshift-weighted field is shown as a dotted line Figure 11. Within our luminosity range the field luminosity function remains relatively unaltered by the redshift weighting. The comparison with the group luminosity function is qualitatively unchanged.

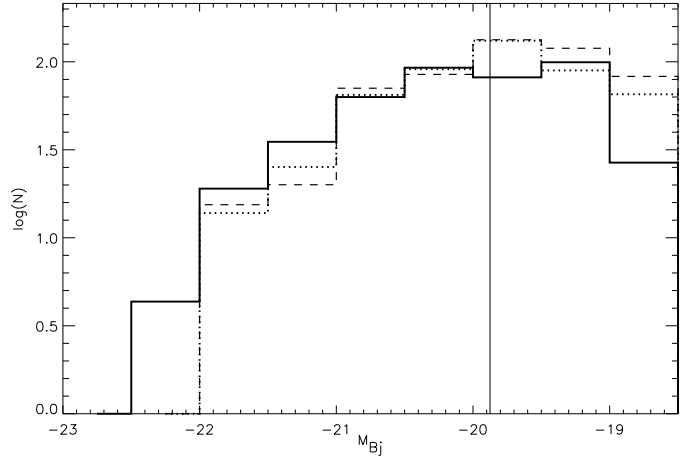


**Figure 11.** The luminosity functions for group (solid line), field (dotted line) and redshift-weighted field (dashed line) galaxies weighted by selection,  $W_C$  and within our redshift range ( $0.3 \leq z \leq 0.55$ ). The vertical line represents the approximate luminosity limits of the sample at the redshift limit  $z = 0.55$ .

Figure 11 suggests that there is an excess of bright galaxies and a deficit of faint galaxies in the groups compared to the field. To investigate the statistical significance of this apparent excess of bright galaxies in groups, we split the luminosity functions into three bins of luminosity: bright ( $M_{B_J} \leq -21.0$ ), control ( $-21.0 \leq M_{B_J} \leq -20.0$ ; which encompasses the local value of  $M_* \sim -20.3$  from Norberg et al. 2002, corrected to  $H_0 = 75 \text{ km s}^{-1} \text{ Mpc}^{-1}$ ) and faint ( $-20.0 \leq M_{B_J} \leq -18.5$ ). We prefer this approach over fitting a Schechter function to the luminosity function, since it avoids degeneracy between the cut-off parameter,  $M_*$ , and the faint-end slope parameter,  $\alpha$ . We define two new indices to measure the relative abundances of galaxies in each of these luminosity bins. The bright-to-faint galaxy ratio,  $R_{(B/F)}$ , is defined as the logarithm of the ratio of galaxies in the bright bin to that in the faint bin. The bright-to-control galaxy ratio,  $R_{(B/C)}$  is similarly the logarithm of the ratio of galaxies in the bright bin to that in the control bin. The values of  $R_{(B/C)}$  and  $R_{(B/F)}$  in the field are shown in Table 4.  $R_{(B/C)}$  only utilises data for which galaxies are brighter than the magnitude limit at all redshifts, while  $R_{(B/F)}$  spans a wider range of luminosity (and thus has more leverage to measure changes in the luminosity function) but requires us to correct by the redshift weighting (ie., to compare with the dotted line in Fig. 11). We estimate the significance of the difference in the field and group ratios by bootstrap resampling two mock samples using the field data-set alone, and comparing the difference between the two resampled values. This indicates the likelihood that the observed difference between the group and the field occurs by random sampling from the same underlying distribution.

A comparison between the group and field luminosity functions can now be made by computing  $R_{(B/C)}$  and  $R_{(B/F)}$ . The result of this process is summarised in Table 4. We compute values of  $R_{(B/C)} = -0.425$  for the group galaxy population and  $R_{(B/C)} = -0.600$  for the field galaxy populations, indicating a larger fraction of bright galaxies in the groups. We compute a difference between the group and field of  $\Delta R_{B/C} = +0.175$ ; however, this result has

**Table 4. Field Luminosity Function Properties:** The bright-to-control ( $R_{(B/C)}$ ) and bright-to-faint ( $R_{(B/F)}$ ) ratios of the galaxy populations in the CNOC2 field:

	$R_{(B/C)}$		$R_{(B/F)}$		
	All	Passive	All	Passive	
	Star	Star	Forming	Forming	
-0.600	-0.401	-0.733	-0.865	-0.525	-1.049

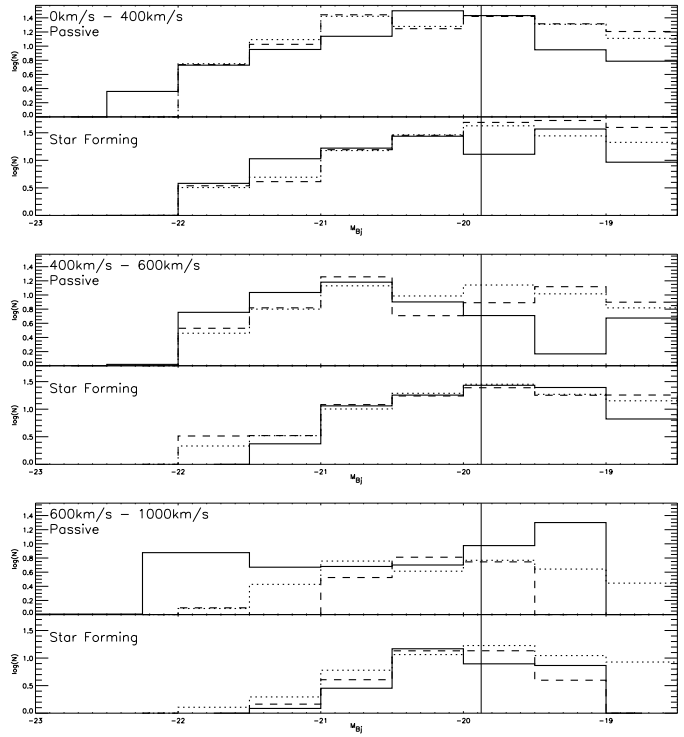
low significance. The computed significance level for the difference  $\Delta R_{B/C}$  is  $S_{B/C} = 85.6$  per cent (there is a  $\sim 15$  per cent chance that the luminosity functions are the same). For  $BF$  we find  $R_{(B/F)} = -0.551$  in the group galaxy population and  $R_{(B/F)} = -0.976$  in the redshift-weighted field population, again indicating a much larger ratio of bright to faint galaxies in the groups than in the field ( $\Delta R_{B/F} = +0.425$ ). In this case, the difference has much higher statistical significance,  $S_{B/F} = 99$  per cent (we can be 99 per cent confident that the difference is real).

Table 5 explores whether the field and group luminosity functions are significantly different for passive and actively star forming types, and whether they differ as a function of group velocity dispersion. Within the uncertainty of the small sample size, the difference in  $R_{(B/F)}$  appears to be evident in both the star forming and passive populations. While the excess of the brightest passive galaxies appears to be most prevalent in the groups with highest velocity dispersion, the depression in the faint galaxy population is most evident in the lower velocity dispersion groups. Only in low velocity dispersion groups is a population of bright star forming galaxies still common. The changing shape of the luminosity function is shown in Figure 12. Figure 13 shows us the dependence on  $\sigma(v)_{intr}$  of the parameters  $\Delta R_{B/C}$  and  $\Delta R_{B/F}$ , graphically depicting the information in Table 5. What is particularly evident in this figure is that whilst the bright, passive galaxies become more important in the high velocity dispersion groups (relative to  $M_*$  galaxies), the bright star forming galaxies become less important. This suggests a bright star forming galaxy population in dense environments may contribute significantly to the formation of the most massive passive galaxies, already highly prevalent in these systems by  $z \sim 0.5$ .

## 7 DISCUSSION AND CONCLUSIONS

We have used the LDSS2 spectrograph on the Magellan telescope at LCO to obtain 418 new galaxy redshifts in the regions of 26 CNOC2 groups at intermediate redshift ( $0.3 \leq z \leq 0.55$ ). Of these, 86 are group members. With the depth of Magellan, we are highly complete and unbiased down to  $R_C = 22.0$  and out to  $240''$  ( $\sim 2r_{200}$  for a  $500 \text{ km s}^{-1}$  group at  $z = 0.3$ ). The primary purpose of this paper is to present this data set.

Our main result of this paper is the significant enhancement of  $f_p$  in our group sample relative to the field level, even in the smallest groups. This indicates that star formation is less prevalent among galaxies in the group environment than in the field, even at intermediate redshift. This could be re-



**Figure 12.** As Figure 11 but with group galaxies split into three bins of velocity dispersion,  $\sigma(v)_{intr}$  going from low  $\sigma(v)_{intr}$  (top panels) to high  $\sigma(v)_{intr}$  (bottom panels); and with star forming and passive galaxies shown separately in the upper and lower panels of each plot.

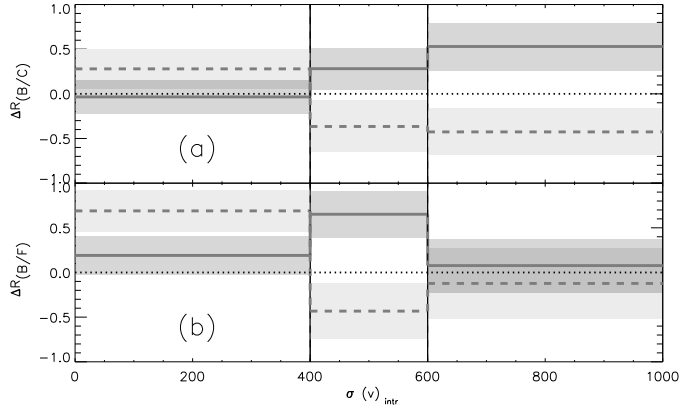


**Figure 13.** The dependence on group velocity dispersion,  $\sigma(v)_{intr}$ , of group luminosity function parameters, normalised by the field, as computed in Table 5. (a) The ratio of bright to control galaxies,  $\Delta R_{B/C}$  and (b) The ratio of bright to faint galaxies,  $\Delta R_{B/F}$ . The solid line represents the passive population, whilst the dashed line represents the star forming population of galaxies. The shaded areas represent the  $1-\sigma$  errors on the parameter, computed using a Monte Carlo technique. These are light grey for the star forming galaxies, darker grey for the passive galaxies, and darker still where the 2 regions overlap. A value of  $\Delta R_{B/C}$  or  $\Delta R_{B/F} = 0$  infers that there is no difference between group and field luminosity functions (dotted line).

**Table 5. Group Luminosity Function properties:** The bright-to-control ( $R_{(B/C)}$ ) and bright-to-faint ( $R_{(B/F)}$ ) ratios of the passive and star forming galaxy populations in the CNOC2 groups and the field. Additional columns give the enhancement of  $R_{(B/C)}$  or  $R_{(B/F)}$  in the groups relative to the field with associated error ( $\Delta R_{B/C} \pm \sigma(\Delta R_{B/C})$ ,  $\Delta R_{B/F} \pm \sigma(\Delta R_{B/F})$ ) and significance of each enhancement ( $S_{B/C}$ ,  $S_{B/F}$ ).

$\sigma(v)_{intr}(\text{km s}^{-1})$	p/sf	$R_{(B/C)}$	$\Delta R_{B/C}$	$\sigma(\Delta R_{B/C})$	$S_{B/C}$	$R_{(B/F)}$	$\Delta R_{B/F}$	$\sigma(\Delta R_{B/F})$	$S_{B/F}$
All	All	-0.425	0.18	0.12	85.6%	-0.971	0.43	0.13	99.0%
All	p	-0.29	0.12	0.16	53.1%	-0.52	0.21	0.18	79.1%
All	sf	-0.64	0.10	0.19	40.4%	-1.14	0.30	0.19	88.8%
0-400	p	-0.434	-0.03	0.19	13.6%	-0.593	0.19	0.22	64.9%
0-400	sf	-0.453	0.28	0.22	80.3%	-1.269	0.69	0.23	99.7%
400-600	p	-0.118	0.28	0.23	78.3%	-0.459	0.65	0.26	97.7%
400-600	sf	-1.098	-0.35	0.29	72.9%	-0.963	-0.43	0.31	78.3%
600-1000	p	0.129	0.53	0.26	95.4%	-0.424	0.08	0.30	20.2%
600-1000	sf	-1.159	-0.41	0.26	91.8%	-0.971	-0.12	0.39	30.6%

lated to either a different formation history in the group environment, intragroup environmental processes accelerating galaxy evolution to the passive state, or a combination of these two effects.

We have investigated how this deficit of star forming galaxies depends on the group properties, and find only relatively weak correlations. Whilst there is little overall trend of  $f_p$  with group velocity dispersion, there is a suggestion that  $f_p$  is higher in the more concentrated systems with  $\sigma(v)_{intr} > 400 \text{ km s}^{-1}$ . We examined the radial dependence of  $f_p$ , finding a weak trend with radius. Comparing  $f_p$  with the nearest neighbour distance, the passive fraction declines significantly at large separations, suggesting a relation to the substructure within groups. Taking into account the low numbers of galaxies in each system, these trends are qualitatively similar to those reported in local group samples (e.g. Hashimoto et al. 1998; Gómez et al. 2003; Girardi et al. 2003; Balogh et al. 2004). The correlations of passive fraction with environment also mimic the dependence of morphology on environment in local groups (e.g. Postman & Geller 1984; Zabludoff & Mulchaey 1998, 2000; Tran et al. 2001).

In rich clusters at the epoch of CNOC2, Fasano et al. (2000) find an evolving fraction of elliptical + S0 galaxy types with a fraction  $f_{E+S0} \sim 0.45 \pm 0.15$  in clusters, within a clustercentric radius of  $0.67h_{75} \text{ Mpc}$  and brighter than  $M_V = -20$ . This is comparable with the mean fraction of passive galaxies in the CNOC2 groups (down to brighter than  $M_{B_J} = -20.0$ , see Figure 7) but with considerably less scatter in these richer systems. We note that the morphology-density relation is also effective in at least some of these clusters (see also Dressler et al. 1997), with a much higher fraction of early-type galaxies (approaching  $f_{E+S0} = 1$ ) in the densest regions. However, the different selection (morphological, V-band limited) and our arbitrary division at  $\text{EW}[\text{OII}] = 5 \text{ \AA}$  makes quantitative comparison difficult. The value of  $f_p$  in groups is also significantly lower than seen in CNOC1 cluster cores at  $z \sim 0.4$ , with mean values of  $f_p \sim 0.7$  within the inner  $0.75h_{75} \text{ Mpc}$  and brighter than  $M_{B_J} = -19.65$  (Nakata et al. 2004, Note: whilst in that paper the division is at  $10 \text{ \AA}$ , we use  $5 \text{ \AA}$  for consistency). In Mulchaey et al., 2005 we will discuss the morphological properties of our sample in detail, using HST ACS imaging (now mostly complete).

We have coadded the data to provide a well under-

stood stacked group sample and a stacked field sample over the same redshift range ( $0.3 \leq z \leq 0.55$ ), and use this sample to investigate the dependence of  $f_p$  on galaxy luminosity. We find that  $f_p$  is greatly enhanced in group galaxies with respect to the field down to at least  $M_{B_J} \sim -19.0$ . In the brightest galaxies ( $M_{B_J} \lesssim -21.0$ ) this trend is strongest in the higher velocity dispersion systems ( $\sigma(v)_{intr} \gtrsim 400 \text{ km s}^{-1}$ ).

We also investigate how the luminosity function of galaxies depends on their environment: local studies have shown that luminosity is at least as important as environment in determining whether a galaxy is passive or star forming at the present day (e.g. Blanton et al. 2004). Our data suggest that the intermediate redshift group galaxy population is enhanced in bright galaxies and that lower velocity dispersion groups ( $\sigma(v)_{intr} \lesssim 400 \text{ km s}^{-1}$ ) have a deficit of faint galaxies compared to the intermediate redshift field. However, only in the more massive groups is the enhanced bright population primarily passive ( $f_p$  also enhanced).

It is instructive to see how these trends compare with similar studies at low redshift in the literature. The variation in the shape of the global luminosity function measured from survey to survey is worryingly large (Driver & De Propris 2003) and so it is important to use data from the same survey where possible in studies of how the luminosity function depends upon environment. Data from SDSS and 2dFGRS suggests that in regions of higher density the local galaxy population is biased towards a brighter characteristic magnitude and steeper faint-end slope (De Propris et al. 2003; Blanton et al. 2003; Croton et al. 2004). This density dependence appears to be dominated by the relative abundance of early-type passive galaxies and may not be obvious in each individual cluster (e.g. the Coma cluster, Mobasher et al. 2003). In local groups there may also be a correlation between group velocity dispersion and the faint-end slope, driven by the population of faint, early type galaxies (Zabludoff & Mulchaey 2000; Christlein 2000). The large population of faint passive galaxies in our most massive groups ( $\sigma(v)_{intr} \gtrsim 600 \text{ km s}^{-1}$ , see Figure 12) suggests that we might be seeing the same trends at  $z \sim 0.45$ , although there appears to be a deficit of faint galaxies in less massive groups, relative to the field. The generation of this

faint passive galaxy population is relavent to downsizing in the red sequence of cluster galaxies, with recent observations indicating that it does not extend faintwards of  $\sim M_* + 2$  at  $z \sim 1$  (Kodama et al. 2004; De Lucia et al. 2004).

In Paper II we will compare our CNOC2 groups to a low redshift group sample selected from the 2dFGRS survey. In Paper III we will examine the morphological composition of our groups, extending studies of the morphology-density relation to group environments at  $z \sim 0.45$ .

## 8 ACKNOWLEDGEMENTS

We would like to thank the staff of the Magellan telescope for their tremendous support. RGB is supported by a PPARC Senior Research Fellowship. DJW, MLB and RJW also thank PPARC for their support. We are grateful to Dan Kelson for the use of his spectral reduction software and to David Gilbank for his help when learning to use it. We also acknowledge *noao* for the wealth of IRAF tools used during data reduction. We also acknowledge Tom Shanks and Phil Outram for their observations at Magellan and the full CNOC2 team for the outstanding dataset. Finally, we thank the anonymous referee for some useful feedback which has helped to improve this paper.

## REFERENCES

Allington-Smith, J. R., Ellis, R., Zirbel, E. L., & Oemler, A. J. 1993, *ApJ*, 404, 521

Baldry, I. K., Glazebrook, K., Brinkmann, J., Ivezić, Ž., Lupton, R. H., Nichol, R. C., & Szalay, A. S. 2004, *ApJ*, 600, 681

Balogh, M., Eke, V., Miller, C., Lewis, I., Bower, R., Couch, W., Nichol, R., Bland-Hawthorn, J., Baldry, I. K., Baugh, C., Bridges, T., Cannon, R., Cole, S., Colless, M., Collins, C., Cross, N., Dalton, G., de Propris, R., Driver, S. P., Efstathiou, G., Ellis, R. S., Frenk, C. S., Glazebrook, K., Gomez, P., Gray, A., Hawkins, E., Jackson, C., Lahav, O., Lumsden, S., Maddox, S., Madgwick, D., Norberg, P., Peacock, J. A., Percival, W., Peterson, B. A., Sutherland, W., & Taylor, K. 2004, *MNRAS*, 348, 1355

Beers, T. C., Flynn, K., & Gebhardt, K. 1990, *AJ*, 100, 32

Blanton, M. R., Eisenstein, D. J., Hogg, D. W., Schlegel, D. J., & Brinkmann, J. 2004, *ApJ*, submitted, astro-ph/0310453

Blanton, M. R., Hogg, D. W., Bahcall, N. A., Baldry, I. K., Brinkmann, J., Csabai, I., Eisenstein, D., Fukugita, M., Gunn, J. E., Ivezić, Ž., Lamb, D. Q., Lupton, R. H., Loveday, J., Munn, J. A., Nichol, R. C., Okamura, S., Schlegel, D. J., Shimasaku, K., Strauss, M. A., Vogeley, M. S., & Weinberg, D. H. 2003, *ApJ*, 594, 186

Bower, R. G. & Balogh, M. L. 2004, in *Clusters of Galaxies: Probes of Cosmological Structure and Galaxy Evolution*, 326–+

Brinchmann, J., Charlot, S., White, S. D. M., Tremonti, C., Kauffmann, G., Heckman, T., & Brinkmann, J. 2004, *MNRAS*, 351, 1151

Butcher, H. & Oemler, A. 1984, *ApJ*, 285, 426

Carlberg, R. G., Yee, H. K. C., Morris, S. L., Lin, H., Hall, P. B., Patton, D. R., Sawicki, M., & Shepherd, C. W. 2001, *ApJ*, 552, 427

Christlein, D. 2000, *ApJ*, 545, 145

Croton, D. J., Farrar, G. R., Norberg, P., Colless, M., Peacock, J. A., Baldry, I. K., Baugh, C. M., Bland-Hawthorn, J., Bridges, T., Cannon, R., Cole, S., Collins, C., Couch, W., Dalton, G., De Propris, R., Driver, S. P., Efstathiou, G., Ellis, R. S., Frenk, C. S., Glazebrook, K., Jackson, C., Lahav, O., Lewis, I., Lumsden, S., Maddox, S., Madgwick, D., Peterson, B. A., Sutherland, W., & Taylor, K. 2004, astro-ph/, in press:, astro

De Lucia, G., Poggianti, B. M., Aragón-Salamanca, A., Clowe, D., Halliday, C., Jablonka, P., Milvang-Jensen, B., Pelló, R., Poirier, S., Rudnick, G., Saglia, R., Simard, L., & White, S. D. M. 2004, *ApJL*, 610, L77

De Propris, R., Colless, M., Driver, S. P., Couch, W., Peacock, J. A., Baldry, I. K., Baugh, C. M., Bland-Hawthorn, J., Bridges, T., Cannon, R., Cole, S., Collins, C., Cross, N., Dalton, G. B., Efstathiou, G., Ellis, R. S., Frenk, C. S., Glazebrook, K., Hawkins, E., Jackson, C., Lahav, O., Lewis, I., Lumsden, S., Maddox, S., Madgwick, D. S., Norberg, P., Percival, W., Peterson, B., Sutherland, W., & Taylor, K. 2003, *MNRAS*, 342, 725

Dressler, A. 1980, *ApJ*, 236, 351

Dressler, A., Oemler, A. J., Couch, W. J., Smail, I., Ellis, R. S., Barger, A., Butcher, H., Poggianti, B. M., & Sharples, R. M. 1997, *ApJ*, 490, 577

Dressler, A. & Shectman, S. A. 1987, *AJ*, 94, 899

Driver, S. & De Propris, R. 2003, *Astrophysics and Space Science*, 285, 175

Efron, B. 1982, *The Jackknife, the Bootstrap and other resampling plans* (CBMS-NSF Regional Conference Series in Applied Mathematics, Philadelphia: Society for Industrial and Applied Mathematics (SIAM), 1982)

Eke, V. R., Baugh, C. M., Cole, S., Frenk, C. S., Norberg, P., Peacock, J. A., Baldry, I. K., Bland-Hawthorn, J., Bridges, T., Cannon, R., Colless, M., Collins, C., Couch, W., Dalton, G., de Propris, R., Driver, S. P., Efstathiou, G., Ellis, R. S., Glazebrook, K., Jackson, C., Lahav, O., Lewis, I., Lumsden, S., Maddox, S., Madgwick, D., Peterson, B. A., Sutherland, W., & Taylor, K. 2004, *MNRAS*, 348, 866

Fasano, G., Poggianti, B. M., Couch, W. J., Bettoni, D., Kjærgaard, P., & Moles, M. 2000, *ApJ*, 542, 673

Flores, H., Hammer, F., Elbaz, D., Cesarsky, C. J., Liang, Y. C., Fadda, D., & Gruel, N. 2004, *A&A*, 415, 885

Gómez, P. L., Nichol, R. C., Miller, C. J., Balogh, M. L., Goto, T., Zabludoff, A. I., Romer, A. K., Bernardi, M., Sheth, R., Hopkins, A. M., Castander, F. J., Connolly, A. J., Schneider, D. P., Brinkmann, J., Lamb, D. Q., SubbaRao, M., & York, D. G. 2003, *ApJ*, 584, 210

Girardi, M., Rigoni, E., Mardirossian, F., & Mezzetti, M. 2003, *A&A*, 406, 403

Hashimoto, Y., Oemler, A. J., Lin, H., & Tucker, D. L. 1998, *ApJ*, 499, 589

Hickson, P., Kindl, E., & Auman, J. R. 1989, *ApJS*, 70, 687

Hopkins, A. M. 2004, ArXiv Astrophysics e-prints

Hopkins, A. M., Miller, C. J., Nichol, R. C., Connolly, A. J., Bernardi, M., Gómez, P. L., Goto, T., Tremonti, C. A., Brinkmann, J., Ivezić, Ž., & Lamb, D. Q. 2003, *ApJ*, 599, 971

Huchra, J. P. & Geller, M. J. 1982, *ApJ*, 257, 423

Jansen, R. A., Franx, M., & Fabricant, D. 2001, *ApJ*, 551, 825

Jones, L. R., McHardy, I., Newsam, A., & Mason, K. 2002, *MNRAS*, 334, 219

Kauffmann, G., White, S. D. M., Heckman, T. M., Ménard, B., Brinchmann, J., Charlot, S., Tremonti, C., & Brinkmann, J. 2004, *MNRAS*, 314

Kelson, D. D. 2003, *PASP*, 115, 688

Kennicutt, R. C. 1992, *ApJS*, 79, 255

Kodama, T., Smail, I., Nakata, F., Okamura, S., & Bower, R. G. 2001, *ApJL*, 562, L9

Kodama, T., Yamada, T., Akiyama, M., Aoki, K., Doi, M., Furusawa, H., Fuse, T., Imanishi, M., Ishida, C., Iye, M., Kajisawa, M., Karoji, H., Kobayashi, N., Komiyama, Y., Kosugi, G., Maeda, Y., Miyazaki, S., Mizumoto, Y., Morokuma, T., Nakata, F., Noumaru, J., Ogasawara, R., Ouchi, M., Sasaki, T., Sekiguchi, K., Shimasaku, K., Simpson, C., Takata, T., Tanaka, I., Ueda, Y., Yasuda, N., & Yoshida, M. 2004, *MNRAS*, 350, 1005

Kurtz, M. J. & Mink, D. J. 1998, *PASP*, 110, 934

Lilly, S. J., Le Fevre, O., Hammer, F., & Crampton, D. 1996, *ApJL*, 460, L1+

Lin, H., Yee, H. K. C., Carlberg, R. G., Morris, S. L., Sawicki, M., Patton, D. R., Wirth, G., & Shepherd, C. W. 1999, *ApJ*, 518, 533

Madau, P., Pozzetti, L., & Dickinson, M. 1998, *ApJ*, 498, 106

Martínez, H. J., Zandivarez, A., Domínguez, M., Merchán, M. E., & Lambas, D. G. 2002, *MNRAS*, 333, L31

Mobasher, B., Colless, M., Carter, D., Poggianti, B. M., Bridges, T. J., Kranz, K., Komiyama, Y., Kashikawa, N., Yagi, M., & Okamura, S. 2003, *ApJ*, 587, 605

Mulchaey, J. S., Davis, D. S., Mushotzky, R. F., & Burstein, D. 2003, *ApJS*, 145, 39

Nakata, F., G., B. R., Balogh, M. L., & J., W. D. 2004, *MNRAS*, accepted

Norberg, P., Cole, S., Baugh, C. M., Frenk, C. S., Baldry, I., Bland-Hawthorn, J., Bridges, T., Cannon, R., Colless, M., Collins, C., Couch, W., Cross, N. J. G., Dalton, G., De Propris, R., Driver, S. P., Efstathiou, G., Ellis, R. S., Glazebrook, K., Jackson, C., Lahav, O., Lewis, I., Lumsden, S., Maddox, S., Madgwick, D., Peacock, J. A., Peterson, B. A., Sutherland, W., & Taylor, K. 2002, *MNRAS*, 336, 907

Poggianti, B. M., Smail, I., Dressler, A., Couch, W. J., Barger, A. J., Butcher, H., Ellis, R. S., & Oemler, A. J. 1999, *ApJ*, 518, 576

Postman, M. & Geller, M. J. 1984, *ApJ*, 281, 95

Ramella, M., Geller, M. J., & Huchra, J. P. 1989, *ApJ*, 344, 57

Ramella, M., Pisani, A., & Geller, M. J. 1997, *AJ*, 113, 483

Ramella, M., Zamorani, G., Zucca, E., Stirpe, G. M., Vettolani, G., Balkowski, C., Blanchard, A., Cappi, A., Cayatte, V., Chincarini, G., Collins, C., Guzzo, L., MacGillivray, H., Maccagni, D., Maurogordato, S., Merighi, R., Mignoli, M., Pisani, A., Proust, D., & Scaramella, R. 1999, *A&A*, 342, 1

Schlegel, D. J., Finkbeiner, D. P., & Davis, M. 1998, *apj*, 500, 525

Severgnini, P. & Saracco, P. 2001, *Astrophysics and Space Science*, 276, 749

Shepherd, C. W., Carlberg, R. G., Yee, H. K. C., Morris, S. L., Lin, H., Sawicki, M., Hall, P. B., & Patton, D. R. 2001, *ApJ*, 560, 72

Strateva, I., Ivezić, Ž., Knapp, G. R., Narayanan, V. K., Strauss, M. A., Gunn, J. E., Lupton, R. H., Schlegel, D., Bahcall, N. A., Brinkmann, J., Brunner, R. J., Budavári, T., Csabai, I., Castander, F. J., Doi, M., Fukugita, M., Győry, Z., Hamabe, M., Hennessy, G., Ichikawa, T., Kunszt, P. Z., Lamb, D. Q., McKay, T. A., Okamura, S., Racusin, J., Sekiguchi, M., Schneider, D. P., Shimasaku, K., & York, D. 2001, *AJ*, 122, 1861

Tonry, J. & Davis, M. 1979, *AJ*, 84, 1511

Tran, K. H., Simard, L., Zabludoff, A. I., & Mulchaey, J. S. 2001, *ApJ*, 549, 172

Tucker, D. L., Oemler, A. J., Hashimoto, Y., Shectman, S. A., Kirshner, R. P., Lin, H., Landy, S. D., Schechter, P. L., & Allam, S. S. 2000, *ApJS*, 130, 237

Whitaker, R. J., Morris, S. L., & The CNOC2 Team. 2004, *MNRAS*, in preparation

Wilman, D. J., Balogh, M. L., Bower, R. G., Mulchaey, J. S., Oemler Jr, A., Carlberg, R. G., Eke, V. R., Lewis, I. J., Morris, S. L., & Whitaker, R. J. 2004, *MNRAS*, accepted

Wilson, G., Cowie, L. L., Barger, A. J., & Burke, D. J. 2002, *AJ*, 124, 1258

Yee, H. K. C., Ellingson, E., & Carlberg, R. G. 1996, *ApJS*, 102, 269

Yee, H. K. C., Morris, S. L., Lin, H., Carlberg, R. G., Hall, P. B., Sawicki, M., Patton, D. R., Wirth, G. D., Ellingson, E., & Shepherd, C. W. 2000, *ApJS*, 129, 475

Zabludoff, A. I. & Mulchaey, J. S. 1998, *ApJ*, 496, 39

—. 2000, *ApJ*, 539, 136

## APPENDIX A: COMPLETENESS IN THE STACKED GROUP

Despite the greater depth and spectroscopic completeness achieved in the region of the groups with our Magellan targeting, it was still necessary to adopt a sparse sampling strategy due to the high density of targets, especially close to our new magnitude limit of  $R_c = 22$ . In this section, we investigate the selection functions for the spectroscopic sample, seeking a representative means of stacking the data. The CNOC2 photometric catalogue is complete to  $R_c \sim 23$  and so the probability that we possess a redshift of any galaxy brighter than this limit can be easily understood. In Section A1 we assume that our Magellan data reach sufficient depth to be unbiased at magnitudes  $R_c \leq 22$ . We then describe a simple weighting scheme which accounts for targeting bias in both CNOC2 and Magellan spectroscopic samples. This scheme differentiates between galaxies with redshifts from each source which have different selection functions. In Section A2 we test our assumption of unbiased redshift completeness in the Magellan data and show that this assumption holds within the limits of tests using current data.

### A1 Selection Functions

To understand the selection functions for the spectroscopic sample, it must first be split into its component CNOC2 and

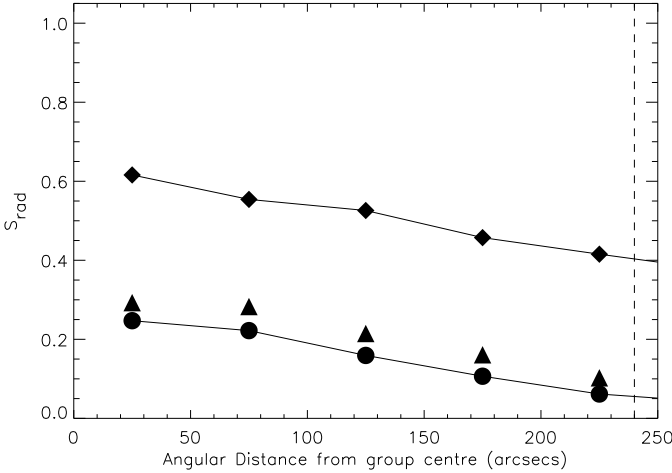


**Figure A1.** Radial selection function of the stacked data as a function of angular distance from the target group centre. Filled circles represent the fraction of galaxies with Magellan redshifts ( $S_{rad}(L_z)$ ); triangles represent the fraction of galaxies targetted by Magellan ( $S_{rad}(L_{obs})$ ) and diamonds represent galaxies with CNOC2 or Magellan redshifts ( $S_{rad}(L_z) + S_{rad}(C_z)$ ). Only galaxies within  $240''$  and with  $R_C \leq 22.0$  are considered in our analysis.

Magellan subsets as selection depends critically on the observing strategies and facilities used. Target selection in the CNOC2 spectroscopic survey was primarily dependent upon apparent  $R_c$ -band magnitude. However, below the nominal spectroscopic limit of  $R_c = 21.5$  in that survey, galaxies with redshifts become biased towards strong EW[OII] with respect to those obtained using Magellan. In contrast target selection with Magellan is dependent upon both magnitude and angular distance from the targetted group centre. However there appears to be no strong bias towards emission redshifts brighter than our magnitude limit of  $R_c = 22$  (see Section A2). Therefore we can implement a simple weighting scheme which simulates a 100 per cent complete survey and removes targetting bias and CNOC2 redshift incompleteness bias simultaneously:

The weighting scheme requires a radial selection function and a magnitude-dependent selection function. For each galaxy in the spectroscopic sample, a radial weight  $W_{rad}$  and a magnitude-dependent weight,  $W_{mag}$  are computed in such a way that the total weight of all galaxies with redshifts (measured-z galaxies)  $\sum_1^{N_{spec}} (W_{rad} \cdot W_{mag}) = N_{phot}$ , the total number of galaxies in the photometric sample brighter than  $R_c = 22$ . We denote galaxies with redshifts from the original CNOC2 survey with the suffix ( $C_z$ ) and those with Magellan LDSS2 redshifts with the suffix ( $L_z$ ).

We begin by looking at the radial selection function,  $S_{rad}$ . The fraction of galaxies with CNOC2 redshifts shows no significant dependence upon angular distance from the centre of the nearest group and so we choose  $W_{rad}(C_z) = 1$  for all these galaxies. However there is a strong dependence on angular radius for the fraction of Magellan redshifts (or Magellan targets). In Figure A1, the fraction of galaxies in the CNOC2 photometric catalogue ( $R_c \leq 22$ ) targetted by Magellan,  $S_{rad}(L_{obs})$  (triangles), where redshifts were obtained,  $S_{rad}(L_z)$  (filled circles) and including the fraction with CNOC2 redshifts,  $S_{rad}(L_z) + S_{rad}(C_z)$  (diamonds) is

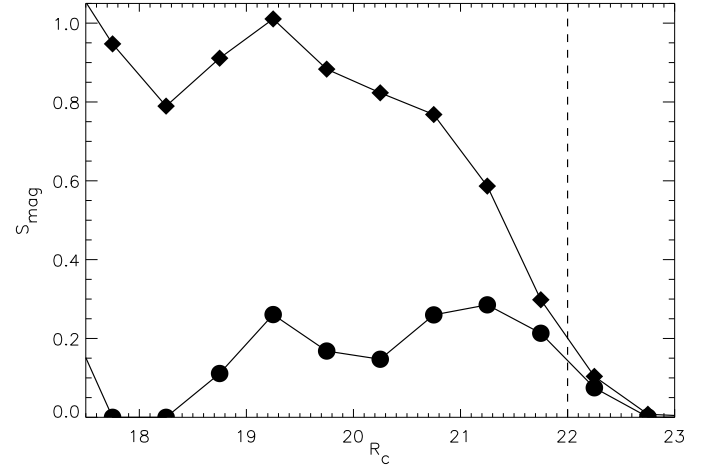


**Figure A2.** Selection functions of the stacked group sample as a function of  $R_c$ -band magnitude. Filled circles represent the fraction of galaxies with Magellan redshifts, weighted by  $W_{rad}$  ( $S_{mag}(L_z)$ ) and diamonds represent galaxies with CNOC2 or Magellan redshifts ( $S_{mag}(L_z) + S_{mag}(C_z)$ ). Only galaxies brighter than  $R_c = 22$  are considered in our analysis.

shown as a function of angular radius. Most untargetted galaxies lie in the magnitude range  $21.5 \leq R_c \leq 22$ . We apply a final cut to stacked data at  $240''$  which is the approximate limiting radius for LDSS2 targetting. This corresponds to  $1h_{75}^{-1}$  Mpc at the low redshift end of our sample,  $z = 0.3$ . The linear spline through the filled circles ( $S_{rad}(L_z)$ ) represents the radial selection function  $S_{rad}(L_z)$  from which the value of  $S_{rad}$  is linearly interpolated for any galaxy targetted with Magellan. For these galaxies, the radial weight is then simply computed to be  $W_{rad}(L_z) = S_0(L_z)/S_{rad}(L_z)$ , normalised so that galaxies located at the group centre receive a weighting  $W_{rad} = 1$ . We note that a galaxy at  $240''$  receives a weighting of  $W_{rad} \sim 4.47$ .

In Figure A2, we show the magnitude-dependent selection function. Galaxies are limited to within  $240''$  and galaxies with redshifts are weighted by  $W_{rad}$ . As in Figure A1, we plot the fraction of galaxies with Magellan redshifts,  $S_{mag}(L_z)$  (filled circles) and the fraction with Magellan or CNOC2 redshifts,  $S_{mag}(L_z) + S_{mag}(C_z)$  (diamonds).  $W_{mag}$  must weight the galaxies such that  $\sum_1^{N_{spec}} (W_{rad} \cdot W_{mag}) = N_{phot}$  in each magnitude bin and the combined weight of all galaxies must accurately emulate the properties of the entire galaxy population. In each bin of magnitude we normalise the total weighted fraction of CNOC2 redshifts to be equal to the fraction of CNOC2 redshifts in the unweighted sample,  $S_{mag}(C_z)$ . We know that in the entire population, that fraction at least will have the properties of CNOC2 spectroscopic galaxies, regardless of CNOC2 redshift incompleteness. Magellan targets come from the remaining galaxies without CNOC2 redshifts (ignoring a tiny comparison sample) and these have properties typical of that population at any given magnitude (based upon our assumption of unbiased redshift completeness in the Magellan data - see Section A2). Therefore the remainder of the combined weight required to match the total number of galaxies in any magnitude bin ( $N_{phot}$ ) is spread amongst the galaxies with Magellan redshifts. Thus  $W_{mag}$  is computed independently for galaxies with CNOC2 redshifts and Magellan redshifts

using equations A1 and A2, below (which simplify to equations A3 and A4). We note that each quantity is computed at a given  $R_c$ -band magnitude (or across each magnitude bin).

$$W_{mag}(C_z) = 1 + \frac{[N_{phot} - N_{C_z} - \Sigma(W_{rad}(L_z))]}{N_{phot}}, \quad (A1)$$

where  $W_{mag}(L_z) = 1 + \alpha$  and

$$\alpha = \frac{[N_{phot} - N_{C_z} - \Sigma(W_{rad}(L_z))]}{N_{phot}} \times \frac{N_{phot} - N_{C_z}}{\Sigma(W_{rad}(L_z))}. \quad (A2)$$

In terms of  $S_{mag}(C_z)$  and  $S_{mag}(L_z)$  these become:

$$W_{mag}(C_z) = 1 + [1 - S_{mag}(C_z) - S_{mag}(L_z)] \quad (A3)$$

and  $\alpha$  in equation A2 becomes:

$$\alpha = [1 - S_{mag}(C_z) - S_{mag}(L_z)] \times \frac{1 - S_{mag}(C_z)}{S_{mag}(L_z)}, \quad (A4)$$

where  $S_{mag}(C_z)$  and  $S_{mag}(L_z)$  are computed by linear interpolation through the points in Figure A2. The combined weight for each galaxy is then given by

$$W_C = W_{rad} \times W_{mag}. \quad (A5)$$

We note from Figure A2 that in the magnitude bin at  $21.5 \leq R_c \leq 22$  the fraction of galaxies with redshifts is down to  $\sim 30$  per cent. However, it is at magnitudes below  $R_c = 21$  that the Magellan data comes to dominate the statistics and the greater depth of the larger telescope allows us to achieve unbiased and highly successful redshift determination down to  $R_c = 22$ . This fainter galaxy population is expected to be more star forming than the brighter population in the local Universe (e.g. Brinchmann et al. 2004). Therefore by reaching this depth, we can begin to probe the evolution of group galaxy properties since intermediate redshift significantly below  $M_*$  to reach this interesting population of mainly star forming galaxies.

## A2 Magellan Redshift Completeness

To investigate redshift incompleteness in the galaxies targeted with Magellan, we examine the distribution of targeted galaxies in colour-magnitude  $((B - R_c), R_c)$  space (Figure A3). If there were a bias associated with preferentially losing absorption-line (early-type) galaxies, then one would expect those galaxies for which we could not measure redshifts to be clustered mainly towards the red end of the colour range. In Figure A3 we compare the colour and magnitude distributions of objects for which we could not measure redshifts (bottom panel - hereafter referred to as lost objects) with those for which we have emission redshifts (top panel) and absorption redshifts (centre panel). We restrict this analysis to fainter than  $R_c = 19.5$  where not all targets are successful. Open symbols represent objects with redshifts outside our range of interest,  $0.3 \leq z \leq 0.55$  or below the luminosity range considered in the analysis,  $M_{B_J} \geq -18.5$ . Lost objects are not concentrated in the red ( $B - R_c \gtrsim 2.0$ ), absorption redshift dominated region, as might be expected if we were preferentially losing absorption line ( $\sim$  early type) galaxies. Indeed, the lost galaxies

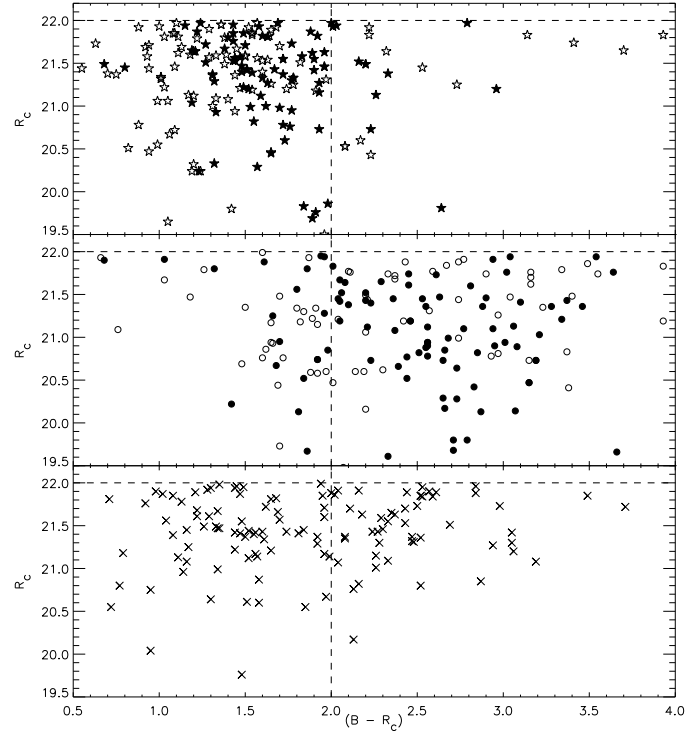


**Figure A3.**  $B - R_c$  colour vs  $R_c$  magnitude for  $R_c \leq 22$  objects targeted with Magellan. The top panel (stars) and middle panel (circles) show the positions of the 187 emission redshift objects and 196 absorption redshift objects in this plane respectively. Filled symbols represent objects which make the redshift and luminosity cuts for our analysis ( $\sim 50$  per cent of all objects in the range  $0.3 \leq z \leq 0.55$ ;  $M_{B_J} \geq -18.5$ ). The bottom panel locates in the colour-magnitude plane the 124 objects targeted with Magellan which failed to yield redshifts. The magnitude limit ( $R_c = 22$ ) and a rough division in colour at  $B - R_c = 2.0$  are also shown (dotted lines).

are spread quite evenly across the full colour range, suggesting no colour bias due to redshift-incompleteness (and thus no bias in star forming properties). Nonetheless, we are cautious in evaluating any such bias as it will impact directly upon our results. Therefore we perform two further checks.

The first check involves making a detailed analysis of the lost objects. We begin by making a manual examination of the spectra for the 19 lost objects with magnitudes  $R_c \leq 21$ . Six of these objects are stars misclassified as galaxies and are removed from the catalogue. A further 10 of the objects have noisy, low signal spectra, which could represent Low Surface Brightness (LSB) galaxies or astrometric offsets from the brightest galaxy regions. Most of these objects have extended morphology, as assessed from the CNOC2 imaging. We also characterize the objects by measuring the signal in a significant part of the spectrum. We measure the combined signal (total counts,  $cts$ ) from the wavelength ranges 5300Å–5530Å and 5645Å–5820Å which span the most efficient region of the grism, eliminating the strong night sky lines. From 13 lost objects with  $cts \geq 3 \times 10^4$ , there are 8 stars, 1 quasar, 1 BL Lac, 1 LSB galaxy, 1 highly noisy spectrum and 1 unclassifiable object. In the low signal range, most objects with  $cts \leq 10^4$  are lost, although there are also some relatively low signal to noise galaxies with clear

absorption redshifts. Finally, lost objects in the intermediate  $10^4 \leq \text{cts} \leq 3 \times 10^4$  range tend to have noisy spectra, often lacking emission lines. However, all blue galaxies ( $B - R_c \lesssim 2.0$ ) with redshifts in this region possess emission lines and so it seems possible that the blue lost objects in this region lie at low redshift where [OII] falls out of the spectral window. Alternatively, it is possible that those galaxies without redshift do not for some reason possess emission lines despite their blue colours. However, red ( $B - R_c \gtrsim 2.0$ ) lost objects with this signal range simply appear noisier and with less obvious absorption features than their counterparts with redshifts.

The second check involves computing a redshift incompleteness weight,  $W_{NoZ}$  which is computed by distributing the weight of the lost object across its five nearest neighbours with redshifts in colour ( $B - R_c$ ) - magnitude ( $R_c$ ) space. Nearest neighbours are computed by equating 1 magnitude in  $R_c$  to 0.5 magnitudes in colour. Then the combined weight of each galaxy is computed to be  $W = W_{rad} \times W_{mag} \times W_{NoZ}$ . We note that Wilson et al. (2002) have performed a similar correction to compensate for galaxies in their sample for which they could not obtain redshifts. In Figure A4 we show the fraction of passive galaxies in the sample  $f_p$  (at  $0.3 \leq z \leq 0.55$ ) as a function of apparent magnitude  $R_c$  without applying this additional weight  $W_{NoZ}$  (solid line) with statistical errors computed using the Jackknife method. We show how this uncorrected version changes when we apply the redshift incompleteness weight ( $W_{NoZ}$ ) to all galaxies (dashed line) and when we apply it to red galaxies only ( $B - R_c \geq 2.0$ , dotted line). The latter correction assumes that all lost blue galaxies lie outside our redshift range whilst lost red galaxies are lost simply due to low signal to noise spectra. This is the most biased scenario we can imagine, yet even in the faintest bin, the difference made to  $f_p$  is comparable with the statistical error. Therefore we consider the LDSS2 redshift incompleteness to be unbiased at  $R_c \leq 22.0$ , to the best of our knowledge.

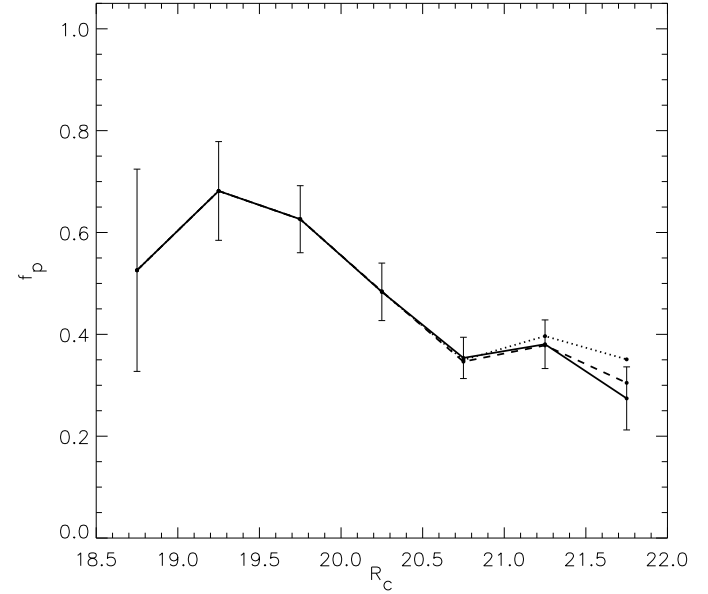


**Figure A4.** The fraction of passive galaxies,  $f_p$  as a function of apparent magnitude for all galaxies in the range  $0.3 \leq z \leq 0.55$ . Galaxies are weighted by  $W_C$  to account for selection bias. The solid line does not make any correction to account for bias in Magellan redshift incompleteness. Jackknife errors are computed in this case. The dashed line represents the case where galaxies with Magellan redshifts have also been weighted by an additional weight  $W_{NoZ}$ , effectively resampling Magellan lost galaxies (no redshifts) in colour-magnitude space. The dotted line case applies this additional weight only to red ( $B - R_c \geq 2$ ) galaxies.